Journal of Molecular Structure 1200 (2020) 127046

Contents lists available at ScienceDirect

Journal of Molecular Structure

journal homepage: http://www.elsevier.com/locate/molstruc

Structural analysis, molecular dynamics and docking calculations of skin protective tripeptide and design, characterization, cytotoxicity studies of its PLGA nanoparticles

Yagmur Kokcu [a], Serda Kecel-Gunduz [b, *], Yasemin Budama-Kilinc [c], Rabia Cakir-Koc [c], Bilge Bicak [a, b], Tolga Zorlu [d, e], Aysen E. Ozel [b], Sevim Akyuz [f]

[a] Institute of Graduate Studies in Sciences, Istanbul University, 34452, Istanbul, Turkey
[b] Istanbul University, Faculty of Science, Physics Department, 34134, Istanbul, Turkey
[c] Faculty of Chemical and Metallurgical Engineering, Department of Bioengineering, Yildiz Technical University, 34220, Istanbul, Turkey
[d] Graduate School of Natural and Applied Science, Yildiz Technical University, 34220, Istanbul, Turkey
[e] Department of Physical Chemistry, Biomedical Research Center (CINBIO), Universidade de Vigo, 36310 Vigo, Spain
[f] Physics Department, Science and Letters Faculty, Istanbul Kultur University, Atakoy Campus, Bakirkoy, 34156, Istanbul, Turkey

ARTICLE INFO

Article history:
Received 4 March 2019
Received in revised form
26 August 2019
Accepted 7 September 2019
Available online 17 September 2019

Keywords:
GHK
PLGA
Nanoparticles
FT-IR
Molecular docking

ABSTRACT

The main purpose of current study is to analyze the structural behaviour of a skin protective tripeptide Gly-His-Lys (GHK) with anti-oxidant and anti-cancer properties, design and characterize its nano-formulation by experimental and spectroscopic techniques to ensure its stability and enhance bioavailability and biocompatibility. GHK is extensively used as a cosmetic products for the therapy of skin and hair deformation. In this study the calculations on GHK were performed at DFT/B3LYP level of theory with the 6−311++G (d,p) basis set to obtain optimized geometry, HOMO-LUMO energy gap, MEP analysis and vibrational wavenumbers. The spectroscopic investigation of GHK tripeptide was performed experimentally through optical spectroscopic techniques (such as *FT-IR, FT-IR-ATR and Micro-RAMAN*) and compared with theoretical wavenumbers. The Potantial Energy Distributions (PED) of the normal modes of vibrations were also carried out with the help of GAR2PED program. By using molecular dynamics simulation, the stability of the GHK in water and methanol mediums have been simulated. To reveal the mechanism of interaction between GHK tripeptide and *Fibroblast Growth Factor*, the hydrogen bonding interactions are also investigated by Molecular docking calculations. Besides, GHK-loaded Poly Lactic-co-Glycolic Acid (PLGA) nanoparticles (NPs) were synthesized with double emission (water/oil/water) method, and characterized with Zeta Sizer, UV−Vis Spectrometry, Transmission Emission Microscope and FT-IR Spectrometry. Due to the encapsulation, the shifts in the wavenumbers occurring at the characteristic peaks of GHK in histidine, peptide and carboxyl groups were also examined. The encapsulation and loading efficiencies were determined as 94% and 4%, also the *in vitro* release profile was performed. Peptide loaded PLGA NPs which have a spherical morphology were visualized by TEM. *In vitro* cell culture studies of both peptide-loaded PLGA NPs and GHK tripeptide were studied and non-toxic effect on L929 cells were found. This study is a pioneer in the development and design of products with nano-drug formulations with better effectiveness and stability, especially in cosmetic products.

© 2019 Elsevier B.V. All rights reserved.

1. Introduction

Glycyl-L-histidyl-L-lysine (GHK) is a tripeptide found in human plasma and saliva, isolated in 1973 by Pickart [1]. There are many important biological properties of this tripeptide. The anti-cancer characteristics of GHK tripeptide which affects the production of RNA in aggressive metastatic colon cancer patients, increases the effects on recovery [2]. GHK or GHK-PEG (GHK-Polyethylene glycol) was found to reactivate apoptosis and inhibit cell growth of human SH-SY5Y neuroblastoma cells and human U937 histiocytic lymphoma cells [3]. GHK's effect on the human gene expression was

* Corresponding author. Physics Department, Science Faculty, Istanbul University, Vezneciler, 34134, Istanbul, Turkey.
E-mail address: skecel@istanbul.edu.tr (S. Kecel-Gunduz).

https://doi.org/10.1016/j.molstruc.2019.127046
0022-2860/© 2019 Elsevier B.V. All rights reserved.

analyzed with the connectivity Map by Pickart et al. It was reported that gene expression changes induced by GHK, and GHK was found to simulate many DNA repair genes [4,5]. The potential therapeutic effects of GHK on fibrotic diseases of the lungs were also obtained by Zhou, X [6]. The anti-oxidant effect of the GHK tripeptide was also examined [7] and found that GHK helps natural protection and prevents the harmful effects of reactive carbonyl species (RCS) and UVB radiation. GHK has also been shown to increase stem cell regeneration in the skin and the potential for rooting and proliferation in epidermal basal cells [8]. It was observed that GHK extinguished the high rate of cytotoxic aldehyde Akrolein (ACR) [9]. GHK also triggers nerve growth, which is an important feature of skin repair. Using neural and glial cells, it was found that GHK increased the growth of neurotrophic factors [10]. The role of GHK in neurons was also investigated by Zhang et al. and demonstrated that GHK alleviated neurological weakness and reduced neuronal apoptosis in the ICH (intracerebral hemorrhage-bleeding in the brain without any trauma effect) rat model [11]. In a study investigating the effects of peptides on regional growth factors and cytokines in regenerative tissues, GHK tripeptide was found to increase the number of axons in nerve cells [12]. The growth of nerve and blood vessels has an important role in skin healing and regeneration, and in a 1994 study, GHK and its derivatives have been shown to induce new vessel growth [13]. In addition, the effects of GHK and GHK analogs on anxiolytic action were also investigated [14]. GHK also tends to be complex in nature due to its molecular structure, in particular the copper complex which allows elderly human liver tissue to synthesize proteins, such as young liver tissue, and is generally studied in the literature [1,15]. In a recent study conducted in 2019, the antibacterial effects of GHK-Cu NPs were demonstrated using *E. coli* and *S. aureus* and the wound healing potentials were verified by the wound scratch assays using L929 dermal fibroblasts [16]. The GHK tripeptide embed PVA nanofiber structers was also synthesized and the structure of nanofibers was examined with SEM, FT-IR and EDX-ray methods. Also the cytotoxicity studies were performed on L929 cells. The authors reported that the non-toxic nanofibers sheds light on future tissue engineering studies [17].

The nano-drug delivery systems provide targeted therapies, as they increase the stability of the drugs or bioactive compounds which they contain as well as minimizing the toxic effects on healthy cells, and are of great importance in terms of revealing their effectiveness in the tissue. The PLGA - poly (lactic co-glycolic acid) - polymer was preferred in this nano drug design, which is the most preferred synthetic polymer due to the fact that the polymer does not emit toxic substances in the environment during cell breakdown and when decomposed, lactic acid, which was turn into carbon dioxide and water is metabolized in the body, and glycolic acid, is also metabolized and excreted via the kidney [18]. In addition, Poly (lactic-co-glycolic acid) is a polymer approved for use in drug delivery systems by the United States Food and Drug Administration (FDA) and the European Medical Agency (EMA) [19].

In this study, nanoparticle (NP) synthesis was performed by using double emission technique. The size, particle distribution, polydispersity index and zeta potential characterizations of the synthesized NPs were obtained by the Zeta sizer device. Encapsulation and loading efficiencies were calculated using the UV−Vis spectrometer and the *in vitro* release profile was extracted. Peptide loaded PLGA NPs which have a spherical morphology were also visualized by TEM analysis results. *In vitro* cell culture studies of GHK and peptide-loaded PLGA NPs were performed and the non-toxic effect on L929 cells were also investigated. In addition, NP characterization was also performed with Dynamic Light Scattering (DLS) for PLGA and GHK-loaded PLGA NPs. By comparing the experimental spectra (*FT-IR, FT-IR-ATR*) of the tripeptide, PLGA polymer and GHK-loaded PLGA NPs, the NP characterization was determined and the peaks shifted due to the encapsulation were identified using band component analysis method.

In silico methods enable to simulate the basic biochemical processes by quantum mechanical, molecular dynamics and molecular docking calculations. Molecular docking calculations provide us to simulate the atomic level interaction between a ligand and a receptor and, thus the binding mechanism of the small molecules in the binding (active) region of the targeted proteins can be characterized. The Fibroblast growth factor was chosen as the target protein in docking calculations, as it showed potential effects for the repair and regeneration of tissues. GHK also triggered nerve growth, which is an important feature of skin repair. ADME (absorption, distribution, metabolism and excretion) profile is substantial for drug candidates, which characterize the drug levels and the kinetics of drugs acting on the tissues and the efficacy and pharmacological activity. In this study, using Schrödinger package program, the ADME profile of the GHK tripeptide was carried out using the Qik-Prop tool, and the distribution and absorption values in different tissues were determined and its potential for being able to be a drug was revealed. Although there are many important studies in the literature that prove the anticancer, antioxidant and anti-inflammatory properties of GHK and reveal its effect in the field of health, there is no studies based on GHK's nano-drug design were found. Therefore, the main objective of this study was to prepare and characterize GHK-loaded PLGA NPs to increase the stability of the GHK tripeptide in the body and to provide controlled release in the region where it will act.

2. Materials and methods

2.1. Materials

The GHK tripeptide ($C_{16}H_{28}N_6O_6$), whose molecular weight was 400.43 g/mol, was purchased commercially at Active Peptide with 99% purity. PLGA (lactide:glicolide = 50:50, M_w ~ 38−54 kDa) and poly(vinyl alcohol) (PVA) were purchased from Sigma-Aldrich (St. Louis, USA). Dichloromethane was also provided with Merck Millipore (>99.5%) (Darmstadt, Germany). Ultrapure water was obtained using the Millipore MilliQ Gradient System. DMEM-F12 Medium, Fetal Bovine Serum and Penicilum−Streptomycin were obtained from Gibco. L929 (mouse fibroblast cells) are commercially available from ATTC (https://www.lgcstandards-atcc.org/products/all/CCL-1.aspx?geo_country=tr), and ethical approval is not necessary for the standard cell lines. All the chemicals and solvents were of analytical grade.

2.2. Nanoparticle preparation method

Using the double emulsion (w/o/w) method, blank PLGA and GHK-PLGA-NPs were prepared. Different concentrations of GHK-loaded PLGA NPs were synthesized from the optimized PLGA NP formulation. PLGA was dissolved in 2 mL DCM. Different amounts of GHK (0.25; 0.5; 1; 1.5; 2.0; 2.5; 3; 5; 10; and 20 mg) were added aqueous solution separately. These solutions were sonicated at 75 W for 4 min. Then 4 mL of 2.5% PVA solution was added separately, and sonicated at 75 W for 4 min. The mixture was left overnight under continuous stirring for removing DCM. Next day, obtained GHK-loaded PLGA NPs were washed three times to remove any residual organic solvent. The supernatant was removed and the pellet was dissolved by completion with 10 mL of distilled water on the pellet. To obtain NPs at the end of the procedure, NPs were filtered using a 0.45 μm regenerated cellulose membrane.

2.3. Determination of encapsulation and loading efficiency

First, a standard GHK curve was obtained using the Nanodrop Spectrometer (220 nm). The encapsulation efficiency of GHK-PLGA-NPs was determined via Equation (1) and loading efficiency was calculated with Equation (2).

$$\text{Encapsulation Efficiency} = \frac{\text{Total amount of GHK} - \text{Free amount of GHK}}{\text{Total amount of GHK}} \times 100 \quad (1)$$

$$\text{Loading Efficiency} = \frac{\text{Encapsulated amount of GHK}}{\text{Total Nanoparticle Weight}} \times 100 \quad (2)$$

2.4. Dynamic Light Scattering (DLS) and zeta potential analysis

Using Zetasizer Nano ZS (Malvern Instruments, UK) instrument equipped with a 4.0 mV He−Ne laser (633 nm) at a temperature of 25 °C, the size, polydispersity index (PdI), size distribution, and zeta potential of blank PLGA NPs and GHK-loaded PLGA NPs were determined. Before every measurement, each sample was filtered with 0.45-μm regenerated cellulose membrane (Sartorius, Germany) filters to remove the aggregates from the solutions. The measurements of PLGA NPs loaded with 0.25, 0.5, 1.0, 1.5, 2.0, 2.5, 3.0, 5.0, 10.0 and 20.0 mg GHK, which were synthesized using 2.5% PVA and 150 mg PLGA, were obtained and tabulated. The NP (5 mg GHK loaded) which has optimal size and zeta potantial, was used in the calculation of encapsulation and loading efficiency as well as FT-IR ATR and TEM characterization analyzes.

2.5. In vitro release study

The release profiles of GHK, GHK-loaded PLGA NPs were achieved for one set of preparations and re-dispersed in 50 mL PBS buffer (pH = 7.4) at 37 °C under gentle agitation. The *in vitro* release study was performed at time intervals of 0, 0.5, 1, 2, 3, 4, 5, 6, 7, 8, 24 and 48 h. At certain time intervals, the intake amounts of GHK in loaded PLGA NPs were first extracted in PBS solution and then samples were measured spectrophotometrically using UV−Vis spectrometer.

The amount of GHK released (% release) was calculated by the following equation:

$$\text{Release } (\%) = \frac{\text{Released GHK}}{\text{Total GHK}} \times 100 \quad (3)$$

2.6. Transmission electron microscopy (TEM) analysis

The morphology of blank and GHK-loaded PLGA NPs were analyzed at 80 kV using transmission electron microscopy (JEOL TEM 1400 Plus). **TEM** images were obtained by placing the samples in an ultrasound bath for 1−2 min at room temperature and placing two or three drops of the solution on a copper grid with a Formvar-coated carbon support.

2.7. Fourier transform infrared (FT-IR) spectroscopy analysis

The infrared spectroscopic analyses of GHK, PLGA and GHK-PLGA-NPs were performed to determine the functional and characteristic groups, and based on the results of the compared spectra, encapsulation characterization and shifted wavenumber values were determined and compared with the literature values. Analyses were carried out by using both transmission and reflection techniques. The FT-IR transmission spectra were recorded on a Jasco 6300E FT-IR spectrometer, by preparing KBr discs. About 1 mg of the ground sample powder was mixed with 100 mg of KBr and pressed into a pellet. In the case of reflection technique FT-IR-ATR spectra of the samples were recorded using an Attenuated Total Reflection (ATR) unit with a diamond ATR crystal. In addition, the GHK peaks underlying the PLGA polymer peaks were determined by band component analysis method.

2.8. Molecular dynamics (MD) simulation analysis

Molecular Dynamic Simulation was performed using the GROMACS software (version 5.1.2) [20] to determine the conformational change in the water medium on the optimized geometry, calculated at DFT/B3LYP level of theory with the 6−311++ G (d,p) basis set, of the GHK in the vacuum medium obtained by the Gaussian 09 software program [21]. Initially, the GROMOS96 43a1 force field [22] was chosen where the topology file would be created to perform a 10 ns molecular dynamic simulation. GHK tripeptide was placed at the center, a dictance of 1.0 nm between the outside of the molecule and the edge of the solvent box, and simulated with different mediums (water and methanol). The cubic box was filled with 944 mol of SPC (simple point charge) water [23] and 444 mol of methanol for water and methanol mediums, respectively. For both simulations, two Na^+ and three Cl^- ions were added in the cubic box to neutralize the system. After, the steepest descent method was chosen for the energy minimization at 200 ps and 100 ps, for water and methanol mediums, respectively. To equilibrate the temperature and pressure of the systems, NVT (50 ps) and NPT (500 ps) ensembles were carried out for 300 K temperature using a V-rescale thermostat [24] and 1 bar pressure using the isotropic Parrinello-Rahman barostat [25]. To obtain the trajectory files during 10 ns for analysis the systems behaviours, Molecular dynamics (MD) simulations were performed by applying periodic boundary conditions in all three directions. Leap-frog algorithm was used in equation of motion was united in order to generate time-dependent trajectories. All bond lengths were constrained with the LINCS (linear constraint solver) algorithm [26]. The Particle Mesh Ewald (PME) method [27] was used to calculate the long-range electrostatic interaction with a grid width of 0.16 nm and a fourth order cubic interpolation. Verlet cut-off scheme [28] was used with a 0.8 nm cut-off radius for identified the cut-off distances, the van der Waals and the short-range electrostatic interactions. The atom coordinates, velocities and energies were saved every step and obtained the trajectory files. The resulting of trajectory files were viewed and analyzed with the VMD software [29].

2.9. HOMO-LUMO and UV–Vis analysis

Experimental UV–Vis absorption spectra of GHK tripeptide in methanol and distilled water mediums were obtained with Shimadzu UV-1280 UV–Vis recording spectrometer. The absorbance values in the 200–700 nm range were measured for 1 mg/mL of dissolved GHK in distilled water and methanol solutions. The theoretical UV–Vis spectra were calculated by Gaussian09 package program using the time-dependent density functional theory (TD-DFT) method based on the B3LYP/6–311++G(d,p) level optimized structure. The highest occupied molecular orbital (HOMO) and lowest unoccupied molecular orbital (LUMO) which are the main orbitals take part in chemical stability is an important tool of quantum chemistry calculations, as well as optical and electric properties and UV–Vis spectra [30]. The difference between HOMO and LUMO, called as band gap, is defined as the chemical stability of the molecule and help to take the information about energy gap (ΔE), the ionization potential (I), the electron affinity (A), the absolute electronegativity (χ), softness (S) and the absolute hardness (η) [31,32]. The frontier molecular orbitals of the form of GHK tripeptide obtained by Gaussian09 package program with TD-DFT/B3LYP/6–311++G(d,p) basis set.

2.10. MEP analysis

The interactions of the atoms in the molecules are determined by the distribution of the electron density within the molecules. The Molecular Electrostatic Potential (MEP) analysis gives the results of reactivity sites for electrophilic and nucleophilic attacks for molecules. MEP analysis provides a visual method to figure out the relative polarity of the molecules. The electrophilic reactivity (relative abundance of electrons) has shown with negative regions, while the nucleophilic reactivity (relative absence of electrons) has defined with positive regions. Different values of the electrostatic potential at the surface are represented by different colors from red to blue. Red represents the lowest electrostatic potential energy value and blue indicates the highest electrostatic potential energy value.

2.11. Molecular docking analysis

The molecular structure of the GHK tripeptide, which was subjected to molecular dynamics simulation in the water medium for 10 ns at GROMACS program [33] introduced to Schrödinger Maestro program for use as a ligand in the calculation of docking. Schrödinger LigPrep module including 2D–3D conversions, generating variations, correction, verification and optimization of the structure was used to prepare ligand to docking analysis [34]. GHK was prepared for docking calculations by the LigPrep tool in the Maestro 11.4 version using the OPLS3 force field [35]. A maximum of 24 stereoisomers were produced for the ligand after the ionization states at pH 7.0 ± 2.0 were selected. Fibroblast growth factor receptor 2 having 334 sequence length (pdb code: 5EG3) [36], and fibroblast growth factor 2 (pdb code: 4OEE), vascular endothelial growth factor receptor 2 (pdb code: 3VO3) and DNA topoisomerase II (pdb code: 1ZXM) as a receptor were prepared with Protein preparation wizard tool [37] in Schrödinger software. Receptors were obtained from the PDB database but due to the lack of residues in the protein structure, the crystal structures were obtained using the SWISS-MODEL server [38]. All waters, metals and ions except protein were deleted from the data file. The polar hydrogens were added to the heavy atoms in the protein. The bond orders were assigned, charges were defined at pH 7.0 and the selected receptor was optimized using PROPKA [39]. The heavy atoms in the receptor were converged by preferring 0.3 Å RMSD and the OPLS3 force field. After the grid was generated using glide grid generation tool, drug candidate molecule was docked to the receptors using Glide SP (standard precision) module of the Maestro version 11.4 [40–42]. Determination of the pharmacokinetic properties of drug candidate molecules is very important for the design and synthesis of drugs with better bioavailability and pharmacokinetic properties. The drug candidate compounds which easily absorbed orally, easily transported to the target region (skin, stomach, blood brain barrier) in the body and easily removed from the body are determined by ADME profiles which are required by the FDA in the drug approval process [43]. The Qik-Prop module (Schrödinger Release 2017-4: QikProp, Schrödinger, LLC, New York, NY, 2017) was used to determine the ADME profile of the drug candidate molecule.

2.12. In vitro cell culture

The L929 (mouse fibroblast) cell lines were cultured in DMEM-F12 medium (10% FBS, 5 μg/mL penicillin-streptomycin). Cells were incubated at 37 °C in a 5% carbon dioxide with humidity. Cell proliferation was observed via inverted microscope daily until the culture reach 80% confluency. After that cells were separated from the flask surface by trypsinization, and centrifuged at 1000 rpm for 5 min. Then, the cell number in the pellet was counted. Briefly, 1 μL from pellet was taken and dyed with trypan blue, counted by hemacytometer and the cell number in mL was calculated by applying the following formula;

$$\text{Number of cells(in mL)} = \text{Dilution Factor} \times \text{Thoma Lam coefficient } (10000) \times \text{Counted Sample Mean} \quad (4)$$

Cells were then used in toxicity assays.

2.13. XTT assay for toxicity

The cells were prepared as 10^5 cells in 1 mL of Dulbecco's Modified Eagle's Medium (DMEM-F12) cell culture medium, then 100 μL of cell solution were seeded in 96 well flat bottom microplate with final density of 1×10^4 cells for each well. Plates were incubated for 24 h for cell growth and surface coating at 37 °C in 5% CO_2 incubator. The PLGA NPs, GHK-loaded PLGA NPs and GHK were added to the cells at different concentrations of 2, 8, 14, 20, 30, 40, 60 and 100 μg/mL and incubation for 24 h ($n = 5$) and distilled water was used as a negative control. Then XTT test was applied. For the preparation of a solution of XTT sodium salt, 4 mg of 2,3-Bis (2-methoxy-4-nitro-5-sulfophenyl)-2H-tetrazolium-5-carboxanilide (XTT), 10 μL of PMS stock were dissolved in 10 mL of cell culture medium and filtered with a 0.45 μm filter. After the cell culture media of the wells were aspirated, 100 μL of XTT solution was added to each well. The plates were incubated for 4 h at 37 °C, and optical density was measured at 450 nm (Lab-Line multiplate reader). By applying the obtained absorbance values, the percentage cell viability were expressed by the following formula;

$$\%\text{cell viability} = \frac{\text{optical density of sample}}{\text{optical density of control}} \times 100 \quad (5)$$

2.14. Statistical analysis

The data obtained from the experimental and control groups were compared using the SPSS program (version 24.0, SPSS Science,

Chicago, IL). Significant differences are indicated by a–d ($p < 0.05$, Tukey's HSD test) among doses at each time point and x–y ($p < 0.05$, Tukey's HSD test) between time points in the same dose column. $p < 0.05$ was accepted as significant in all statistical evaluations.

3. Results and discussion

3.1. DLS and zeta potential results

In Table 1, the particle size, PdI, size distribution, and zeta potential measurements of the blank PLGA and GHK-PLGA-NPs were implemented using a Zetasizer device (Malvern Zetasizer Nano ZS) and listed. The particle size and zeta potential measurements of blank PLGA-NPs and 5 mg GHK-loaded PLGA-NPs are also given in Fig. 1. The blank PLGA-NPs had a narrow size distribution (by volume) of **98.1%**, with 0.084 PdI and a 246.1 nm average particle size with −13.2 mV zeta potential value (Fig. 1a and b), while the GHK-loaded PLGA-NPs (5 mg) had also a narrow size distribution (by volume) of **98%,** with 0.074 PdI and a 223 nm average particle size and −21.4 mV zeta potential value (Fig. 1c and d).

3.2. Determination of encapsulation and loading efficiency of GHK

The standard GHK curve was obtained by a nanodrop device (220 nm) shown in Fig. 2a, the supernatants of NPs were analyzed, the GHK concentration in the supernatant was determined and the encapsulation efficiency was calculated by using Equations (1) and (2), respectively. For the GHK-loaded PLGA NPs and this value was observed to be 94%. The particle weight by freez-dried the loaded NPs, the loading efficiency was calculated as 4% using the equation given above. This means that each 1-mg GHK-PLGA-NP contained 0.04 mg GHK.

3.3. Results of in vitro release study

The *in vitro* release analysis which was taken at time intervals of 0, 0.5, 1, 2, 3, 4, 5, 6, 7, 8, 24 and 48 h was shown in Fig. 2b. Considering the *in vitro* release results obtained at 0, 0.5, 1, 2, 3, 4, 5, 6, 7, 8, 24 and 48 h, when the resulting release graph is interpreted; 50% of the drug was released at the end of the first 7 h, and at the end of the 48th hour, 90% of the drug was released.

3.4. Results of TEM analysis

In Fig. 3, the particle size obtained from the TEM results of blank PLGA NPs and GHK-loaded PLGA NPs were measured at 169 nm and 139.01 nm, respectively. As a result of TEM images, the spherical and non-aggregated morphologies of NPs are clearly obtained from different perspectives.

Table 1
Blank and different amounts of GHK-loaded NPs size, zeta and PdI (Polydispersity Index) values.

PVA (%)	PLGA	Amounts of GHK	Size (nm)	Zeta (mV)	PdI
2.5%	150 mg	Blank PLGA	246.1 ± 82.69	−13.2 ± 5.44	0.084
		0.25 mg GHK	240.8 ± 60.54	−0.783 ± 5.64	0.025
		0.5 mg GHK	222.1 ± 61.27	−1.61 ± 7.59	0.060
		1.0 mg GHK	221.7 ± 53.50	−13.2 ± 7.55	0.009
		1.5 mg GHK	223.6 ± 52.08	−1.65 ± 6.33	0.010
		2.0 mg GHK	227.2 ± 93.58	−7.18 ± 6.42	0.124
		2.5 mg GHK	238.3 ± 83.88	−3.39 ± 4.32	0.108
		3.0 mg GHK	214.7 ± 69.14	−5.98 ± 7.90	0.069
		5.0 mg GHK	223.0 ± 75.10	−21.4 ± 6.21	0.074
		10.0 mg GHK	231.3 ± 78.03	−20.5 ± 6.66	0.064
		20.0 mg GHK	245.8 ± 72.32	−13.5 ± 5.30	0.047

3.5. FT-IR spectroscopy results

In this study, the experimental fundamental vibrational wavenumbers (FT-IR, FT-IR-ATR, Raman) of GHK together with the calculated wavenumbers at the level of DFT-RB3LYP/6–311++G(d,p) basis set, and the assignment of the fundamental vibrational bands in accordance with the potantial energy distribution of the vibrational modes were obtained by Gar2PED program [44] were tabulated at Table 2. The assignments of the specific absorption bands of the GHK tripeptide and PLGA NPs, the observed FT-IR, FT-IR-ATR and Raman spectra were listed at Table 3. The observed FT-IR and ATR spectra of PLGA, GHK and peptide-loaded NPs were plotted comparatively in the range of 1800-400 cm^{-1}, as shown in Fig. 4a and 4b.

3.5.1. PLGA polymer assignments

The strong bands observed in 1759 cm^{-1} in FT-IR and 1754 cm^{-1} and 1753 cm^{-1} in the ATR spectra, are characteristic bands of C = O stretching vibration of the PLGA polymer. These bands in the literature were observed at 1760(IR), 1750(IR), 1750(IR) cm^{-1}, and 1749(IR), 1746(IR) cm $^{-1}$ for dl lactide, glycolide, PLA and PLGA polymer, respectively [45–47].

The asymmetric angular deformation vibrations of the CH_3 and CH_2 groups of PLGA are expected in the range of 1500 - 1250 cm^{-1} [48]. In the FT-IR spectrum for the glycolide and lactide forming PLGA polymer, these vibrations were marked at 1540 cm^{-1} and 1430 cm^{-1} [45]. In the FT-IR spectrum of PLGA NPs (Fig. 4a), these modes were observed at 1455, 1425 and 1395 cm^{-1}, while in the ATR spectrum (Fig. 4b) corresponding vibrations were obtained at 1451, 1424 and 1392 cm^{-1}. In IR spectra of lactide, glycolide monomers and PLA homopolymers; the C–O stretching was obtained at 1275; 1100 cm^{-1}, 1265; 1050 cm^{-1} and 1130; 1090 cm^{-1}, respectively [45]. The peaks, observed in the FT-IR spectrum at 1274; 1092 cm^{-1} and in the ATR spectrum at 1270; 1089 cm^{-1} are the characteristic peaks that define the C–O bond stretching of the PLGA polymer. The absorption peaks that defined the C–H bending motion were observed at 940 cm^{-1} and 750 cm^{-1} [45]. In this study; the peaks at 956; 957 cm^{-1} and 750; 745 cm^{-1} also correspond to the C–H bending of PLGA polymer for FT-IR and ATR spectra, respectively.

3.5.2. PED assignment for amide group

The amide I bands which were observed at 1652 cm^{-1}, 1636 cm^{-1} and 1658 cm^{-1}, 1645 cm^{-1} of GHK tripeptide in the FT-IR and ATR spectrum, calculated at 1653 cm^{-1} with 72% contribution of the C = O bond stretching in the peptide group and 1639 cm^{-1} with 73% contribution of the C = O bond stretching and the 6% contribution of CCN angle bending, according to % PED analysis results, were compatible with experimental results. In the range of 1600 - 1480 cm^{-1}, the angle bending of CNH (40–60%) and CN (18–40%) and also $C^{\alpha}C$ bond stretching (10%) in the peptide group leads to the formation of the absorption which associated with the amide II band [49]. These bands were calculated with %PED calculations at 1597 cm^{-1} (61% CNH and 19% CN) and 1491 cm^{-1} (44% CNH and 29% CN) and observed at 1582 cm^{-1}, 1489 $cm^{-1}$and 1584 cm^{-1}in the FT-IR and ATR spectra, respectively. The Amide III band, which is observed in the range of 1320-1220 cm^{-1}, with lower intensity than other amide bands and consists of N–H in-plane bending (10–40%) and C–H and N–H deformation vibrations combined with C–N bond stretching on the peptide bond, was observed at 1241 cm^{-1} for FT-IR and FT-IR-ATR spectra. All of these assignments are in Table 2.

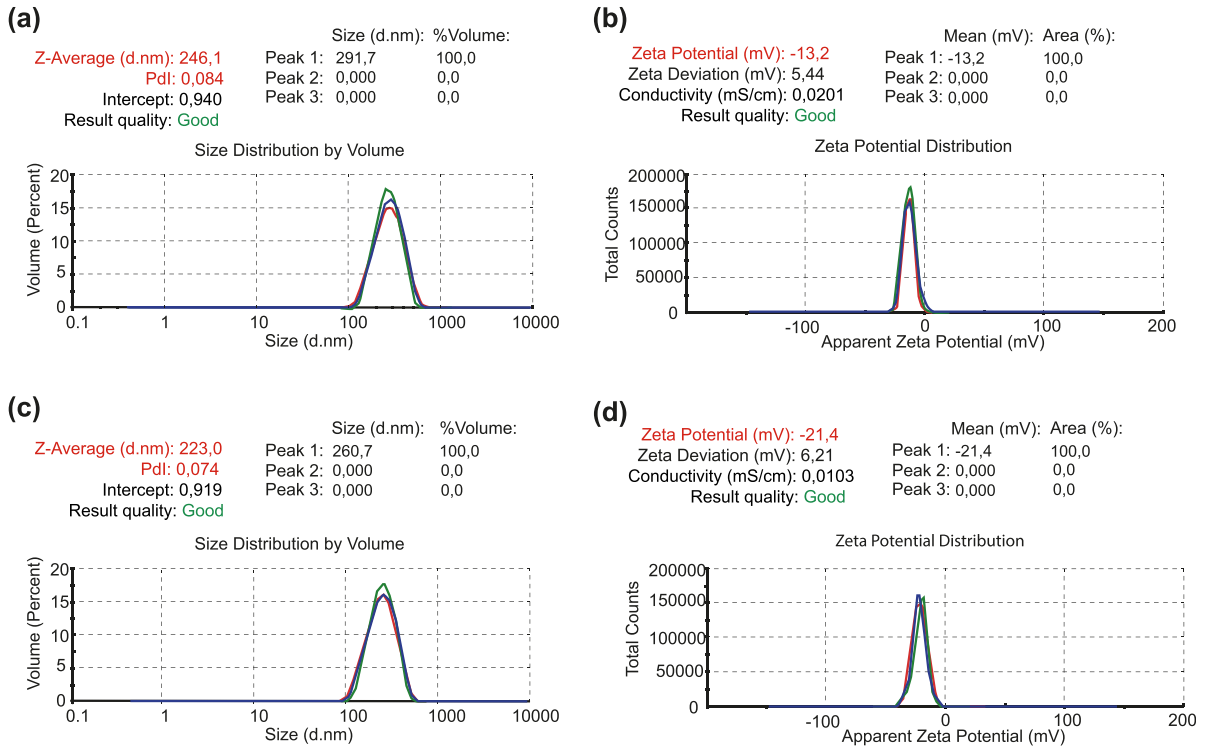

Fig. 1. Size distribution graph (a) and Zeta potential graph of blank PLGA NPs (b). Size distribution graph (c) and Zeta potential graph of GHK-loaded PLGA NPs (d).

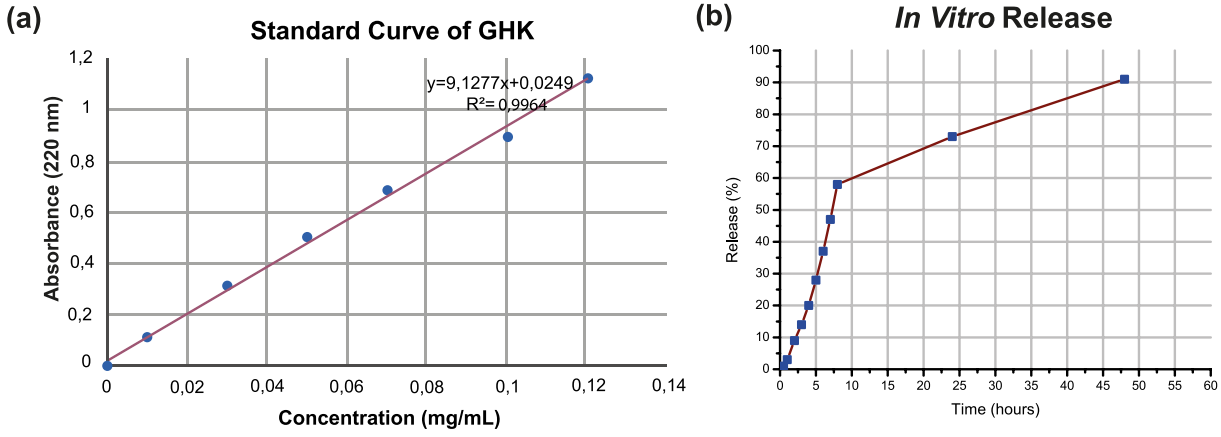

Fig. 2. Standard calibration curve of GHK tripeptide at 220 nm (a). *In vitro* release profile of GHK-loaded PLGA NPs (b).

3.5.3. Shifted wavenumbers

The presence of C = O ester group bands, amide-I, II, III vibrations belonging to amide group, NH_2 amine group, C = C and C = N stretching bands belonging to histidine group and CH_2 group vibrations of GHK which were found between 1700 and 1455 cm^{-1} in the FT-IR and ATR spectra of GHK-loaded NPs, confirming the presence of the drug in NPs and proving that the loading was carried out. Furthermore, the presence of ring torsion and carboxyl group vibrations in the structure of GHK at the ATR spectrum for peptide-loaded NPs in the region of 750-400 cm^{-1} wavenumbers indicated that, the drug is efficiently loaded into NPs. Apart from these, when the drug was loaded into the NP, the shifts in the wavenumbers occurring at the characteristic peaks of the drug were also examined for the first time in this study and tabulated at Table 3. The bond stretching of the C = O ester group in the structure of GHK was observed at 1740 cm^{-1} [50], was recorded at 1733 cm^{-1} in our study in the FT-IR spectrum. In the NP spectrum, this peak is labeled in the FT-IR and ATR spectrum at 1718 cm^{-1} and 1711 cm^{-1}, respectively. In the FT-IR spectra, 1652; 1636 cm^{-1} and the peaks in the ATR spectra 1658; 1645 cm^{-1} were assigned to amide-I vibration belonging to the peptide bonds for GHK, while the peaks at 1652; 1635 $cm^{-1}$and 1659; 1642 cm^{-1} corresponded to amide-I for peptide-loaded NPs, respectively. By applying the band component analysis method to determine the shifted amide-I value for the blank and GHK-loaded NP in ATR spectrum, GHK and peptide-loaded NPs were analyzed in detail and 1645 cm^{-1} and 1642 cm^{-1} which are corresponding to the amide-I vibrations were determined and the shifted value was shown to be 3 cm^{-1} in Fig. 5a.

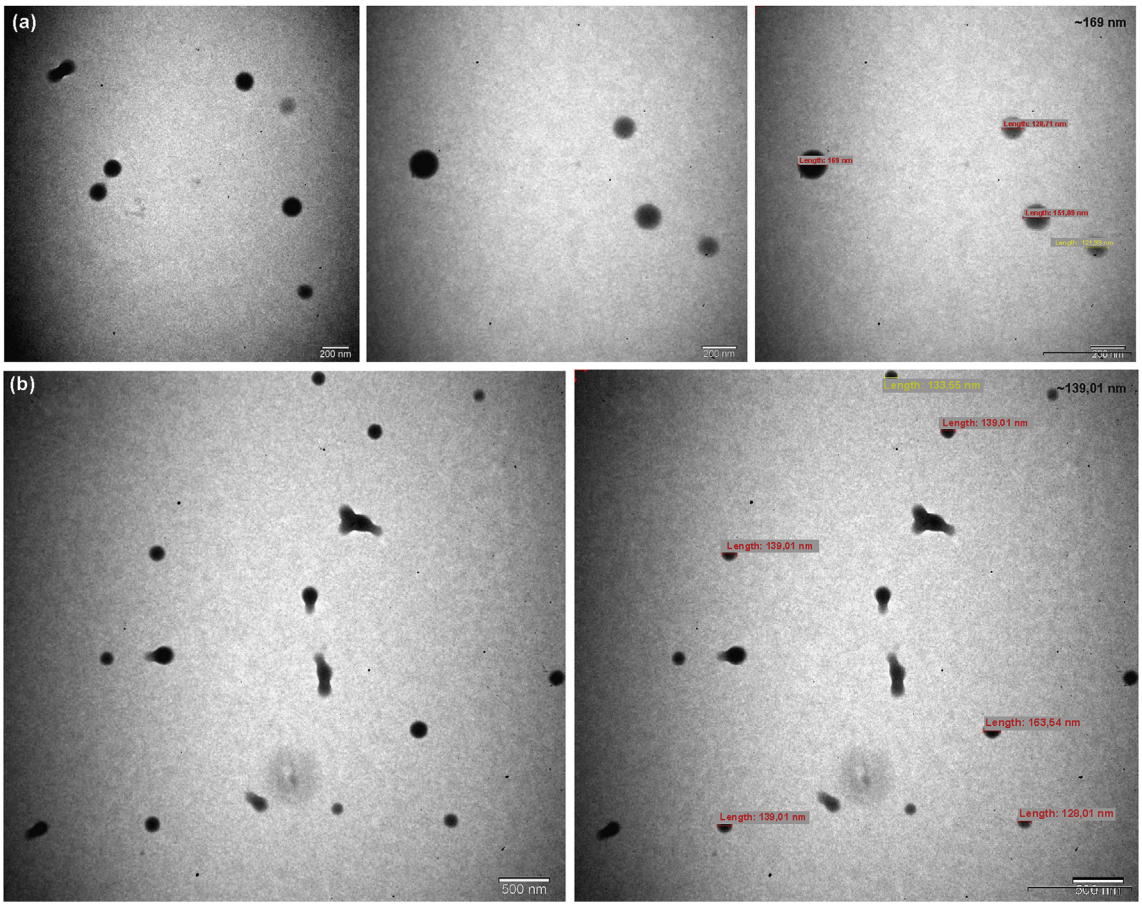

Fig. 3. TEM images of blank PLGA NPs (a) and GHK-loaded PLGA NPs (b).

In the ATR spectra of GHK tripeptide and GHK-loaded PLGA, the interval of the amide II vibration region was examined by band component analysis method in the range of 1611 - 1526 cm^{-1}, and 1593-1558 cm^{-1}, the peaks at 1584 cm^{-1} and 1585 cm^{-1} which are assigned as the amide II for GHK, and GHK-loaded PLGA NP. The peak at 1584 cm^{-1} for GHK was shifted to 1585 cm^{-1} for NP spectrum in Fig. 5b. In order to determine the location of the amide III peak which was masked by the spectrum of the polymer for the loaded NP spectrum, and the amount of shifting value, band component analysis was applied between 1320 cm^{-1} and 1150 cm^{-1} region and the presence of amide III was indicated at 1231 cm^{-1} with very low intensity in Fig. 5c.

The shifts in histidine group vibrations, as well as peptide group were also affected by encapsulation. The C = C and C = N bond stretching wavenumbers were tabulated in Table 3 by shifts close to 1 cm^{-1} and 3 cm^{-1} for histidine moiety. To determine more clearly the shifts of the histidine moiety; the peaks corresponding to the histidine ring vibrations which are hidden under the characteristic polymer spectrum at 1423 cm^{-1}, 1270 cm^{-1},956 cm^{-1} and 746 cm^{-1} in ATR spectrum for GHK-loaded PLGA NPs which agree with angular deformation vibration of the CH_3 and CH_2 groups and C–O stretching and C–H bending of PLGA were investigated by the band component analysis method and the peaks at 1435 cm^{-1}, 1305 cm^{-1}, 1268 cm^{-1} and 947 cm^{-1} are revealed and assigned to $\nu_{CN(ring)}$, $\delta_{CCH(lys)}$, $\nu_{CN(ring)}$ and $\delta_{CNC(ring)}$ modes of GHK, respectively (see Fig S1). In addition, the carboxyl group vibrations of GHK are also affected by encapsulation. The shifts in CCO angle bending and the COOH torsion wavenumbers were 9 cm^{-1}, 4 cm^{-1} and 1 cm^{-1}, respectively and listed at Table 3. In the loaded NP spectrum, the peaks of GHK can be observed in the wavenumber region less than 750 cm^{-1} in the ATR spectrum. The characteristic wavenumbers of the drug which interacts with the polymer have identified for the first time in this study by comparing the spectra between the drug and the GHK-loaded NP.

3.5.4. Comparison of loaded Nanoparticles(5,10,20 mg)

The band, which was observed in the ATR spectrum at 793 cm^{-1} for GHK tripeptide in Fig. 4b and assigned to $\Gamma_{CCNH(peptide)} + \Gamma_{CNCO(peptide)}$ vibration in Table 2 was observed at 788 cm^{-1} for the 5 mg and 10 mg GHK-loaded PLGA spectrum in Fig. S2, but this band not observed for 20 mg GHK-loaded PLGA. For GHK tripeptide, the band that characterized the torsion of the histidine ring in Table 2 was observed at 681 cm^{-1} in Fig. 4b, but only observed for 10 mg GHK-loaded NP spectra at 685 cm^{-1} in Fig. S2. The angle-bending ($\delta_{CCOcarboxyl}$) vibration of the carboxyl group of the GHKin Table 2 was observed at 651 cm^{-1} in Fig. 4b, and this band was detected at 660 cm^{-1} for 5 mg GHK-loaded NP spectrum, but not in the 10 mg GHK -loaded NP spectrum, and at the very low-intensity for 20 mg GHK-loaded NP spectrum in Fig. S2. It has been identified that due to the interaction between the GHK tripeptide and the PLGA polymer, a shift of 9 cm^{-1} was occurred. The band, which was markedly observed for 5 mg GHK-loaded NP spectrum at 645 cm^{-1} in Fig. S2 and characterized the CNCC torsional motion of the histidine ring in Table 2, was recorded with very low intensity at 646 cm^{-1} for 20 mg GHK-loaded NP spectrum. The CONH torsion of the peptide group was obtained at 633 cm^{-1} in the ATR spectrum in Fig. 4b, and this vibrational shift to 2 cm^{-1} and observed at 635 and 631 cm^{-1}, for 5 mg and 20 mg

Table 2
Experimental (FT-IR, Raman and FT-IR-ATR) and calculated wavenumbers (cm^{-1}) and the potantial energy distribution of the vibrational modes of the GHK tripeptide. (The peaks marked as bold-underlined are the peaks obtained as a result of the band component analysis).

	Assign.	This Study				References									This Study			
		GHK				Boc-GHK [50]	GHK [51]		Gly [52]		His [53]		Lys		6-311++G(d,p)			GAR2PED
		IR	Raman		ATR	IR	R	ATR	IR	R	IR	R	IR [54,55]	R [54]	Freq	IR	Raman	%PED
			G	R			G											
		ν_{exp}	ν_{exp}		ν_{exp}	ν_{exp}	ν_{exp}	ν_{exp}	ν_{exp}	ν_{exp}	ν_{exp}	ν_{exp}	ν_{exp}	ν_{exp}	$\nu_{sca.}$	I_{int}	$R_{act.}$	
1	$\nu_{OH(carboxyl)}$				3596								3486		3598	77	140	$\nu_{OH(carboxyl)}(100)$
2	$\nu_{NH(ring)}$														3501	84	188	$\nu_{NH(ring)}(99)$
3	$\nu_{NH(lys)}$												3571		3423	1	88	$\nu_{NH(lys)asy.}(100)$
4	$\nu_{NH(gly)}$	3419							3414						3415	6	35	$\nu_{NH(gly)asy.}(100)$
5	$\nu_{NH(peptide)}$				3363	3373									3391	130	83	$\nu_{NH(peptide)}(99)$
6	$\nu_{NH(lys)}$					3321								3312	3348	1	143	$\nu_{NH(lys)sym}(99)$
7	$\nu_{NH(gly)}$	3288	3286	–	3281										3348	1	102	$\nu_{NH(gly)sym}(100)$
8	$\nu_{NH(lys)}$		3154	–									3198		3175	600	149	$\nu_{NH(peptide)}(99)$
9	$\nu_{CH(ring)}$		3126	–							3165				3136	0	82	$\nu_{CH(ring)}(98)$
10	$\nu_{CH(ring)}$		3111	–							3127	3130			3114	6	73	$\nu_{CH(ring)}(98)$
11	$\nu_{CH(his)}$		2998	–	3003						2984	2987			2984	5	51	$\nu_{CH(his)asy}(99)$
											2956	2960						
12	$\nu_{CH(lys)}$	2953	2956	–	2952									2975	2955	23	90	$\nu_{CH(lys)asy}(91)+\nu_{CH(lys)}(8)$
13	$\nu_{CH(lys)}$														2942	28	13	$\nu_{CH(lys)asym}(90)$
14	$\nu_{CH(lys)}$													2936	2940	39	23	$\nu_{CH(lys)asym}(92)$
15	$\nu_{CH(gly)}$		2936	–					3084	3050					2938	16	51	$\nu_{CH(gly)asym}(99)$
									2920	2930								
16	$\nu_{CH(his)}$	2927	2915	–							2926	2930			2917	19	36	$\nu_{CH(his)sym.}(81)+\nu_{CH(his)}(19)$
17	$\nu_{CH(lys)}$				2905								2871 [54]		2908	17	16	$\nu_{CH(lys)asy}(73)+\nu_{CH(lys)sym}(22)$
18	$\nu_{CH(his)}$														2904	21	95	$\nu_{CH(his)sym}(61)+\nu_{CH(lys)asy}(22)+\nu_{CH(lys)sym}(5)$
19	$\nu_{CH(his)}$														2903	26	172	$\nu_{CH(his)sym}(82)+\nu_{CH(lys)asy}(8)$
20	$\nu_{CH(lys)}$														2898	27	107	$\nu_{CH(lys)sym}(86)+\nu_{CH(lys)asy}(8)$
21	$\nu_{CH(gly)}$														2893	23	128	$\nu_{CH(gly)}(99)$
22	$\nu_{CH(lys)}$														2891	4	82	$\nu_{CH(lys)sym}(75)+\nu_{CH(lys)asy}(20)$
23	$\nu_{CH(lys)}$	2857	2858	–	2857								2868		2878	25	171	$\nu_{CH(lys)sym}(95)$
24	$\nu_{CH(lys)}$		2813	–									2789 [54]		2817	68	111	$\nu_{CH(lys)}(97)$
25	$\nu_{C=O}$	1733	1741	1758		1740			1703	1667			1734 [54]	1734	1729	357	10	$\nu_{C=O(carboxyl)}(80)+\delta_{CCO(carboxyl)}(6)$
													1634					
26	$\nu_{C=O(gly)amide-I}$	1652			1658			1657							1653	92	20	$\nu_{C=O(peptide)amide-I}(72)$
27	$\delta_{HNH(gly)scis}$	1646			1651				1610						1650	25	3	$\delta_{HNH(gly)scis}(94)$
28	$\nu_{C=O(his)amide-I}$	1636	1647	1641	**1645**	1648		1648							1639	397	2	$\nu_{C=O(peptide)amide-I}(73)+\delta_{CCN(peptide)}(6)$
29	$\delta_{HNH(lys)scis}$	1616	1618	1617									1619 [54]		1631	34	3	$\delta_{HNH(lys)scis}(95)$
													1554					
													1525 [54]					
30	$\delta_{CNH(pep)amide-II}$	1582	–	1586	**1584**	1551		1563; 1586							1597	207	3	$\delta_{CNH(peptide)amide-II}(61)+\nu_{CN(peptide)}(19)$
31	$\nu_{C=C(ring)}$	1569	1573	1569	1564		1568; 1569				1575	1573			1570	18	16	$\nu_{C=C(ring)}(50)+\nu_{CC(his)}(13)+\delta_{CCH(ring)}(9)+\delta_{NCH(ring)}(5)$
32	$\nu_{C=N(ring)}$	1497			1496						1490	1490			1496	53	13	$\nu_{C=N(ring)}(39)+\delta_{NCH(ring)}(23)+\nu_{CN(ring)}(6)$
33	$\delta_{HCH(lys)scis}$														1494	8	6	$\delta_{HCH(lys)scis}(84)$
34	$\delta_{CNH(peptide)amide-II}$	1489	1490	1488	–										1491	460	6	$\delta_{CNH(peptide)amide-II}(44)+\nu_{CN(peptide)amideII}(29)+\nu_{CN(his)}(8)$
35	$\delta_{HCH(lys)scis}$	1472	1476	–									1475 [54]		1475	7	4	$\delta_{HCH(lys)scis}(96)$
36	$\delta_{HCH(lys)scis}$	1464			1468								1462 [54]		1465	19	6	$\delta_{HCH(lys)scis}(94)$
37	$\delta_{HCH(lys)scis}$												1445 [54]		1461	4	15	$\delta_{HCH(lys)scis}(95)$
38	$\delta_{HCH(his)scis}$	1457			1455						1451	1451			1450	9	7	$\delta_{HCH(his)scis}(90)$
39	$\delta_{HCH(gly)scis}$	1447	1446	1441					1410	1410					1444	11	8	$\delta_{HCH(gly)scis}(93)$
40	$\nu_{CN(ring)}$	1435			**1435**						1423	1424			1436	30	17	$\nu_{CN(ring)}(40)+\delta_{CNH(ring)}(33)+\delta_{CNC(ring)}(10)$
41	$\delta_{CCH(lys)wagg}$	1404	1408	1404	1405										1403	13	1	$\delta_{CCH(lys)wagg}(72)+\nu_{CC(lys)}(11)+\delta_{CNH(lys)twist}(8)$
42	$\delta_{CCH(lys)wagg}$	1394													1382	5	1	$\delta_{CCH(lys)wagg}(74)+\nu_{CC(lys)}(7)$
43	$\delta_{NCH(gly)}$	1386			1384										1380	8	3	$\delta_{NCH(gly)twist}(44)+\delta_{NCH(his)rock}(13)+$ $\delta_{CCH(his)wagg}(7)+\nu_{CC(gly)}(5)$
44	$\delta_{NCH(gly)}$														1369	11	6	$\delta_{NCH(gly)twist}(25)+\delta_{CCH(his)wagg}(16)+\delta_{NCH(his)rock}(14)$
45	$\delta_{CCH(lys)}$												1355 [54]	1352	1364	4	1	$\delta_{CCH(lys)wagg}(54)+\nu_{CC(lys)}(8)$

46	$\delta_{NCH(lys)}$	1351	1352	–	1352							1356	7	3	$\delta_{NCH(lys)}(40)+\delta_{CCH(lys)twist}(27)$
47	$\delta_{NCH(gly)}$						1334	1323				1342	9	12	$\delta_{NCH(gly)wagg}(41)+\delta_{CCH(his)wagg}(9)+\delta_{CCH(his)}(8)+\delta_{CNH(gly)twist}(6)$
48	$\delta_{COH(carboxyl)}$	1340	1343	1340						1331		1335	41	7	$\delta_{COH(carboxyl)}(18)+\nu_{CO(lys)}(13)+\delta_{CCO(carboxyl)rock}(10)+\delta_{NCH(lys)}(9)+\delta_{NCH(gly)wagg}(8)+\nu_{CC(lys)}(7)$
49	$\nu_{CN(ring)}+\delta_{CCH(his)}$				1334							1335	19	17	$\nu_{CN(ring)}(16)+\nu_{C=N(ring)}(14)+\delta_{CCH(his)twist}(14)+\delta_{NCH(his)}(13)+\delta_{CCH(his)twist}(8)+\delta_{NCN(ring)}(5)$
50	$\delta_{CCH(lys)twist}$	1325			1325					1327 [54]	1326	1322	31	4	$\delta_{CCH(lys)wagg}(15)+\delta_{CCH(lys)twist}(18)+\delta_{COH(karb.)}(7)+\delta_{NCH(gly)wagg}(6)+\delta_{CNH(lys)twist}(6)$
51	$\delta_{NCH(gly)wagg}$											1318	74	13	$\delta_{NCH(gly)wagg}(11)+\delta_{CCH(lys)wagg}(8)+\delta_{CCH(lys)twist}(6)+\delta_{CCH(his)rock}(6)+\delta_{NCH(lys)rock}(6)+\nu_{CC(his)}(6)+\nu_{CN(peptide)}(5)$
52	$\delta_{CCH(lys)}$	1306	1310	1307	**1305**						1309	1310	6	15	$\delta_{CCH(lys)twist}(90)$
53	$\delta_{CCH(his)}$											1296	1	8	$\delta_{CCH(his)wagg}(14)+\delta_{NCH(his)}(14)+\delta_{CCH(lys)}(11)+\delta_{CCH(lys)twist}(17)+\delta_{CCH(lys)wagg}(8)$
54	$\delta_{CCH(his)}$											1295	4	7	$\delta_{CCH(his)wagg}(20)+\delta_{NCH(his)}(16)+\delta_{CCH(lys)rock}(10)+\delta_{CCH(lys)twist}(13)$
55	$\delta_{CCH(lys)}$	1280								1299 [54]		1278	7	6	$\delta_{CCH(lys)twist}(22)+\delta_{CCH(lys)wagg}(11)+\delta_{CNH(lys)wagg}(7)+\delta_{CCH(lys)}(5)$
56	$\nu_{CN(ring)}$	1265	1268	1264	**1268**	1267			1304	1301		1275	22	11	$\nu_{CN(ring)}(18)+\delta_{NCH(ring)}(11)+\nu_{CC(his)}(9)+\nu_{CN(peptide)}(7)+\delta_{CCH(his)twist}(6)+\nu_{CN(his)}(5)$
57	$\delta_{CCH(lys)}$											1258	3	1	$\delta_{CCH(lys)}(26)+\delta_{CCH(lys)wagg}(23)$
58	$\nu_{CN(pep.)amide\ III}$	1241	1246	1239	**1241**							1254	34	2	$\nu_{CN(peptide)amideIII}(16)+\delta_{CCH(his)rock}(11)+\nu_{CN(ring)}(8)$
59	$\delta_{CCH(ring)}$	1225			1224				1265	1262		1224	21	9	$\delta_{CCH(ring)}(26)+\delta_{NCH(ring)}(17)+\nu_{CN(ring)}(17)+\delta_{CCH(his)}(12)$
60	$\delta_{CNH}+\nu_{CN(pep)}$ amide III											1216	48	5	$\delta_{CNH(peptide)}(20)+\nu_{CN(peptide)}(12)+\nu_{CN(his)}(7)+\delta_{NCH(ring)}(7)+\delta_{CCH(ring)}(6)+\delta_{CCH(his)wagg}(6)+\delta_{NHC(his)wagg}(5)$
61	$\delta_{CCH(lys)}$									1186 [54]		1207	0	2	$\delta_{CCH(lys)wagg}(45)+\delta_{CCH(lys)twist}(14)+\delta_{NCH(lys)}(7)+\delta_{CNH(lys)twist}(6)$
62	$\delta_{CCH(his)}$	1185	1188	1185	1187							1176	10	6	$\delta_{CCH(his)twist}(25)+\delta_{CCH(his)rock}(20)+\nu_{CN(his)}(8)+\delta_{NCH(gly)twist}(6)$
63	$\delta_{NCH(gly)}$	1162	1157	1156	1163							1157	67	6	$\delta_{NCH(gly)twist}(35)+\nu_{CO(lys)}(8)+\delta_{COH(carboxyl)}(7)+\delta_{CCH(his)twist}(7)+\nu_{CN(his)}(6)+\delta_{CCH(his)rock}(5)$
64	$\nu_{CO(lys)}$	1150			1153							1156	107	2	$\nu_{CO(lys)}(20)+\delta_{COH(carboxyl)}(7)+\nu_{CC(lys)}(7)$
65	$\delta_{CCH(lys)}$	1142	–	1140	1142					1146 [54]		1145	45	1	$\delta_{CCH(lys)twist}(22)+\nu_{CO(lys)}(12)+\delta_{CNH(lys)twist}(9)+\delta_{COH(carboxyl)}(8)+\nu_{CC(lys)}(7)$
66	$\nu_{CN(lys)}$											1132	12	5	$\nu_{CN(lys)}(15)+\delta_{CCH(lys)rock}(9)+\delta_{NCH(gly)twist}(6)$
67	$\nu_{CN(his)}$	1123	–	1124	1123							1123	5	6	$\nu_{CN(his)}(30)+\delta_{CNH(ring)}(14)+\nu_{CN(gly)}(10)$
68	$\nu_{CN(his)}$					1104						1118	10	5	$\nu_{CN(his)}(22)+\delta_{CNH(ring)}(16)+\nu_{CN(gly)}(16)$
69	$\nu_{CN(gly)}$						1034	1033				1106	5	5	$\nu_{CN(gly)}(20)+\nu_{CN(lys)}(16)+\nu_{CC(lys)}(17)+\delta_{CNH(lys)twist}(5)$
70	$\nu_{CN(his)}$	1090	1097	1093	1089	1086			1087	1085		1081	6	3	$\nu_{CN(his)}(22)+\nu_{CN(gly)}(14)+\nu_{CN(lys)}(7)+\nu_{CC(his)}(6)$
71	$\nu_{CC(lys)}$				1080							1072	9	17	$\nu_{CC(lys)}(73)$
72	$\nu_{CN(his)}$											1070	31	2	$\nu_{CN(his)}(50)+\delta_{CCH(ring)}(26)$
73	$\nu_{CN(lys)}$	1048	1057	1050	1048							1060	8	5	$\nu_{CN(lys)}(60)+\nu_{CC(lys)}(19)$
74	$\nu_{CC(his)}$	1016			1018							1012	11	3	$\nu_{CC(his)}(38)+\delta_{CCN(his)}(8)$
75	$\nu_{CC(his)}$	1005			1007				995	993		1000	0	13	$\nu_{CC(his)}(22)+\delta_{CCH(his)rock}(16)+\delta_{CCC(his)}(21)+\Gamma_{NCCN(his)}(6)$
76	$\nu_{CC(lys)}$											987	4	3	$\nu_{CC(lys)}(23)+\delta_{CCH(his)rock}(6)+\delta_{CCH(lys)twist}(6)+\delta_{CCH(lys)rock}(5)$
77	$\nu_{CC(lys)}$											981	5	6	$\nu_{CC(lys)}(24)+\delta_{CNH(lys)twist}(12)+\delta_{CCC(lys)}(15)+\nu_{CN(lys)}(8)+\delta_{CNC(ring)}(6)$
78	$\delta_{CNC(ring)}$	985	990	986	984				975	975		973	11	4	$\delta_{CNC(ring)}(32)+\nu_{CN(his)}(18)+\nu_{CC(his)}(13)$
79	$\nu_{CC(lys)}$											962	7	1	$\nu_{CC(lys)}(45)+\nu_{CN(lys)}(20)$
80	$\delta_{NCN(ring)}$	948	938		**947**				941	935		940	4	2	$\delta_{NCN(ring)}(54)+\delta_{CNC(ring)}(20)+\delta_{CCH(ring)}(8)$
81	$\nu_{CC(gly)}$	929		932	928							936	32	7	$\nu_{CC(gly)}(17)+\Gamma_{HNCH(gly)}(16)+\delta_{CCH(his)rock}(13)$
82	$\delta_{NCH(gly)}$		–	910	910							900	11	1	$\delta_{NCH(gly)rock}(71)+\Gamma_{CNCO(peptide)}(17)+\Gamma_{HNCH(gly)}(5)$
83	$\Gamma_{HNCH(gly)}$											888	207	2	$\Gamma_{HNCH(gly)}(48)+\nu_{CN(gly)}(20)$
84	$\nu_{CC(lys)}$		883	–								882	10	3	$\nu_{CC(lys)}(15)+\nu_{CO(lys)}(12)+\delta_{CCH(lys)twist}(14)+\delta_{CCH(his)rock}(6)+\delta_{CCH(lys)rock}(6)$
85	$\delta_{CCH(his)}$	874	–	877	875							877	36	7	$\delta_{CCH(his)rock}(23)+\delta_{CCO(his)}(11)+\nu_{CC(lys)}(6)+\nu_{CC(his)}(6)+\delta_{CNC(peptide)}(5)$
86	$\Gamma_{CNHH(lys)}$	838	–	842	837							848	12	1	$\Gamma_{CCNH(lys)}(22)+\delta_{CCH(lys)rock}(10)+\nu_{CC(lys)}(7)+\delta_{CCH(his)rock}(6)$
87	$\delta_{CCH(lys)}$											823	41	1	$\delta_{CCH\ (lys)rock}(28)+\Gamma_{CCNH(lys)}(14)+\nu_{CC(lys)}(12)$
88	$\Gamma_{CNCH(ring)}$	814			816				827			808	12	1	$\Gamma_{CNCH(ring)}(67)+\Gamma_{CCNC(ring)}(13)$
89	$\Gamma_{CNHH(lys)}$				804							805	81	1	$\Gamma_{CCNH(lys)}(38)+\delta_{CCH(lys)rock}(27)+\Gamma_{CNCH(ring)}(7)$
90	Γ_{CCNH}	794			793							794	61	1	$\Gamma_{CCNH(peptide)}(31)+\Gamma_{CNCO(peptide)}(29)+\Gamma_{CNCH(lys)}(6)+\Gamma_{CNCH(ring)}(5)$
91	$\Gamma_{CNCH(ring)}$	777	781	772	776				764			779	10	1	$\Gamma_{CNCH(ring)}(18)+\Gamma_{CNCN(ring)}(16)+\delta_{CCC(his)}(10)+\nu_{CC(his)}(7)+\delta_{CNC(ring)}(7)+\Gamma_{CCNC(ring)}(6)+\delta_{NCN(ring)}(5)$
92	$\Gamma_{NCCH(ring)}$											757	20	1	$\Gamma_{NCCH(ring)}(32)+\Gamma_{NCCN(his)}(15)+\Gamma_{NCCN(ring)}(13)+\Gamma_{CCNC(ring)}(7)$
93	$\delta_{CCH(lys)}$	740	–	742	739							740	2	0	$\delta_{CCH(lys)rock}(71)$
94	$\Gamma_{NCCH(ring)}$				724							726	8	3	$\Gamma_{NCCH(ring)}(33)+\nu_{CC(gly)}(8)+\delta_{CCH(his)rock}(6)+\delta_{NCC(gly)}(5)$
95	$\Gamma_{CCOH(carboxyl)}$	720	–	714	715							715	36	5	$\Gamma_{CCOH(carboxyl)}(46)+\nu_{CC(lys)}(16)+\delta_{CCO(carboxyl)}(5)$
96	$\Gamma_{NCCH\ (ring)}$	681			681							708	5	1	$\Gamma_{NCCH(ring)}(14)+\Gamma_{NCCN(ring)}(11)+\Gamma_{NCCN(his)}(11)+\delta_{CCO(gly)rock}(9)+\delta_{NCC(gly)}(8)+\Gamma_{CCNC(ring)}(6)+\Gamma_{NCCN(gly)}(6)+\nu_{CC(gly)}(5)$

(*continued on next page*)

Table 2 (*continued*)

	Assign.	This Study				References									This Study			
		GHK				Boc-GHK [50]	GHK [51]		Gly [52]		His [53]		Lys		6-311++G(d,p)			GAR2PED
		IR	Raman		ATR	IR	R	ATR	IR	R	IR	R	IR [54,55]	R [54]	Freq	IR	Raman	%PED
			G	R			G											
		ν_{exp}	ν_{exp}		ν_{exp}	ν_{exp}	ν_{exp}	ν_{exp}	ν_{exp}	ν_{exp}	ν_{exp}	ν_{exp}	ν_{exp}	ν_{exp}	$\nu_{sca.}$	I_{int}	$R_{act.}$	
97	$\Gamma_{NCCN(ring)}$				670						664	660			666	12	1	$\Gamma_{NCCN(ring)}(38)+\nu_{CC(his)}(8)+\Gamma_{CCNC(ring)}(6)$
98	$\delta_{CCO(carboxyl)}$	652	–	656	651										649	55	1	$\delta_{CCO(carboxyl)}(21)+\Gamma_{CCOH(carboxyl)}(14)+\delta_{NCC(lys)}(7)+\delta_{CCC(lys)}(14)+\nu_{CC(his)}(5)$
99	$\Gamma_{CNCC(ring)}$														643	5	1	$\Gamma_{CCNC(ring)}(51)+\Gamma_{NCCN(ring)}(5)$
100	$\Gamma_{CONH(peptide)}$		633	–	633										632	39	1	$\Gamma_{CONH(peptide)}(29)+\Gamma_{CNCC}(18)+\Gamma_{CNCH(his)}(13)+\Gamma_{NCCN(gly)}(5)+\delta_{NCH(gly)rock}(5)$
101	$\Gamma_{CNCC(ring)}$	616		621	615						619				624	11	2	$\Gamma_{CCNC(ring)}(28)+\Gamma_{NCCN(his)}(13)+\nu_{CC(his)}(7)+\Gamma_{CCOH(carboxyl)}(7)+\delta_{CCO(his)}(5)$
102	δ_{CCN}				588										586	11	1	$\delta_{CCN}(20)+\delta_{CCO(carboxyl)}(12)+\delta_{CCC(his)}(7)+\Gamma_{CCOH(carboxyl)}(7)+\delta_{CCC(lys)}(6)+\delta_{CCN}(6)$
103	$\Gamma_{COOH(carboxyl)}$	570	–	573	575				584						567	62	1	$\Gamma_{COOH(carboxyl)}(53)+\delta_{CCO(carboxyl)}(12)+\delta_{CCC(lys)}(5)$
104	$\Gamma_{NCCN(gly)}$				547										540	46	1	$\Gamma_{NCCN(gly)}(30)+\Gamma_{CNCC(his)}(23)+\delta_{NCH(gly)rock}(11)+\delta_{CCO(his)rock}(7)+\Gamma_{CONH(peptide)}(7)$
105	$\Gamma_{NCNH(ring)}$	520	–	526	534										526	92	1	$\Gamma_{NCNH(ring)}(66)+\Gamma_{CCNC(ring)}(28)$
106	$\delta_{CCO(carboxyl)}$	506	–	507	499										496	15	2	$\delta_{CCO(carboxyl)}(16)+\delta_{CCN}(10)+\delta_{CCC(his)}(8)$
107	$\delta_{CCC(lys)}$	448	–	449	446										454	4	1	$\delta_{CCC(lys)}(48)+\delta_{CCH(lys)rock}(8)+\nu_{CC(lys)}(6)$
108	$\delta_{CCN(lys)}$	429	–		436										428	12	1	$\delta_{CCN(lys)}(49)+\delta_{CCC(lys)}(18)+\nu_{CC(lys)}(6)$
109	$\delta_{CCC(his)}$	406			411										408	14	1	$\delta_{CCC(his)}(30)+\delta_{CCN(ring)}(15)+\delta_{NCC(his)}(7)$
110	$\delta_{CCO(his)}$	399		399	401										378	10	1	$\delta_{CCO(his)rock}(18)+\delta_{NCC(lys)}(16)+\delta_{CNC}(13)+\delta_{CCC(lys)}(11)+\Gamma_{CCOH(carboxyl)}(7)+\delta_{NCC(his)}(6)+\delta_{CCH(lys)}(5)$
111	δ_{CCN}		–	340											346	2	1	$\delta_{CCN}(21)+\delta_{CCO(carboxyl)}(8)+\delta_{CCC(his)}(7)+\delta_{NCC(lys)}(6)$
112	$\Gamma_{NCCH(his)}$														321	29	2	$\Gamma_{NCCH(his)}(33)+\delta_{CCN(ring)}(12)+\delta_{CCC(his)}(8)$
113	$\delta_{CCN(ring)}$														318	3	3	$\delta_{CCN(ring)}(18)+\delta_{CCO(carboxyl)}(12)+\Gamma_{NCCC(his)}(12)+\delta_{NCC(his)}(6)+\nu_{CC(his)}(6)$
114	$\delta_{CCN(ring)}$		–	300											303	15	1	$\delta_{CCN(ring)}(13)+\Gamma_{NCCC(his)}(12)+\delta_{NCC(lys)}(7)+\delta_{CCO(carboxyl)}(6)$
115	$\delta_{NCC(gly)}$														283	12	1	$\delta_{NCC(gly)}(16)+\delta_{CCN}(11)+\Gamma_{HNCH(gly)}(9)+\Gamma_{CCNC(ring)}(7)+\delta_{NCC(lys)}(5)$
116	$\delta_{CCC(lys)}$		–	271											279	3	1	$\delta_{CCC(lys)}(18)+\delta_{CCC(his)}(8)+\delta_{CCN(ring)}(6)+\delta_{CCO(carboxyl)}(6)+\Gamma_{NCCC(his)}(6)$
117	$\Gamma_{CCNH(lys)}$														254	56	0	$\Gamma_{CCNH(lys)}(80)$
118	$\Gamma_{HNCH(gly)}$														241	8	4	$\Gamma_{HNCH(gly)}(13)+\delta_{CCC(lys)}(8)+\Gamma_{CCCH(lys)}(7)+\delta_{CCC(his)}(7)+\delta_{CCN}(5)$
119	$\Gamma_{HNCH(gly)}$														225	34	1	$\Gamma_{HNCH(gly)}(33)+\delta_{CCC(lys)}(22)$
120	$\Gamma_{HNCH(gly)}$														214	24	0	$\Gamma_{HNCH(gly)}(27)+\delta_{CCC(lys)}(11)+\delta_{CCN}(7)+\delta_{NCC(gly)}(6)+\delta_{CCC(his)}(6)$
121	$\delta_{CCC(his)}$														198	3	0	$\delta_{CCC(his)}(34)+\delta_{CCC(lys)}(14)+\delta_{CCN(ring)}(6)$
122	$\Gamma_{NCCH(his)}$														152	1	1	$\Gamma_{NCCH(his)}(25)+\delta_{CNC}(13)+\delta_{CCC(his)}(11)$
123	$\delta_{CCC(lys)}$														140	2	1	$\delta_{CCC(lys)}(40)+\Gamma_{NCCH(his)}(7)+\delta_{CCN(lys)}(6)$
124	$\delta_{CCC(his)}$														135	1	1	$\delta_{CCC(his)}(18)+\Gamma_{CCNC(ring)}(15)+\Gamma_{NCCO(his)}(15)+\delta_{CNC}(9)+\Gamma_{CNCC}(5)$
125	$\Gamma_{CCCH(lys)}$		–	126											124	2	0	$\Gamma_{CCCH(lys)}(68)+\delta_{CCC(lys)}(8)$
126	$\Gamma_{CNCO(his)}$		–	89											92	5	1	$\Gamma_{CNCO(his)}(43)+\Gamma_{CNCC}(15)+\Gamma_{CONH(peptide)}(15)+\Gamma_{CNCH(his)}(6)$
127	Γ_{CNCC}														81	1	1	$\Gamma_{CNCO(peptide)}(14)+\Gamma_{CNCC}(24)+\delta_{CNC}(9)+\Gamma_{NCCO(gly)}(7)$
128	$\Gamma_{CCCH(lys)}$														77	3	0	$\Gamma_{CCCH(lys)}(61)+\Gamma_{CNCO(peptide)}(7)$
129	$\Gamma_{CONH(peptide)}$		–	76											74	5	0	$\Gamma_{CONH(peptide)}(38)+\Gamma_{NCCO(gly)}(9)+\delta_{NCC(his)}(8)+\Gamma_{CCCH(lys)}(7)+\Gamma_{CNCC}(5)$
130	$\Gamma_{NCCO(his)}$														64	1	1	$\Gamma_{NCCO(his)}(19)+\Gamma_{CNCO(peptide)}(15)+\delta_{CCN}(7)+\Gamma_{CCCN(his)}(14)+\delta_{CNC}(7)$
131	$\Gamma_{NCCO(gly)}$														57	2	0	$\Gamma_{NCCO(gly)}(32)+\Gamma_{CONH(peptide)}(12)+\Gamma_{CNCC(his)}(7)$
132	$\Gamma_{CCCN(his)}$														50	3	1	$\Gamma_{CCCN(his)}(45)+\Gamma_{CCCH(lys)}(6)+\Gamma_{NCCO(lys)}(6)+\Gamma_{CONH(peptide)}(6)+\Gamma_{CNCH}(5)$
133	$\Gamma_{NCCC(his)}$														46	3	1	$\Gamma_{NCCC(his)}(31)+\Gamma_{NCCO(lys)}(23)+\Gamma_{NCCO(gly)}(10)+\Gamma_{CONH(peptide)}(6)+\delta_{CCC(his)}(5)$
134	$\Gamma_{NCCC(his)}$														42	1	1	$\Gamma_{NCCC(his)}(50)+\Gamma_{NCCO(his)}(8)+\Gamma_{NCCO(gly)}(8)+\delta_{CCC(his)}(13)$
135	$\Gamma_{CNCH(lys)}$														31	1	0	$\Gamma_{NCCH(lys)}(44)+\Gamma_{NCCO(lys)}(16)+\Gamma_{CCCH(lys)}(15)$
136	$\Gamma_{NCCO(his)}$														27	1	2	$\Gamma_{NCCO(his)}(39)+\Gamma_{CCCN(his)}(25)+\Gamma_{CNCC(his)}(8)+\Gamma_{NCCO(lys)}(8)$
137	$\Gamma_{CNCO(peptide)}$														22	0	1	$\Gamma_{CNCO(peptide)}(28)+\Gamma_{NCCO(his)}(18)+\Gamma_{CCCN(his)}(10)+\Gamma_{CNCC}(8)$
138	$\Gamma_{CNCH(lys)}$														8	1	2	$\Gamma_{CNCH(lys)}(41)+\Gamma_{NCCO(lys)}(29)+\Gamma_{NCCO(his)}(7)$

Table 3
The observed FT-IR, FT-IR-ATR and Raman spectra and assignments of GHK and GHK-loaded PLGA NPs.(The peaks marked as underlined are the peaks obtained as a result of the band component analysis, the peaks marked with * are the peaks of the PLGA.).

												This Study					
		pH 6.8 GHK [51]		pH 8.9 GHK [51]								GHK				GHK-PLGA NP	
	Boc-GHK [50]	GHK		GHK		Glycine [52]		Histidine [53]		Lysine		RAMAN		FT-IR	ATR	FT-IR	ATR
	FT-IR	Raman	ATR	Raman	ATR	Raman	FT-IR	Raman	FT-IR	Raman [54]	FT-IR [54,55]	Green	Red				
NH(gly)asym												–	–	3419	–	3420	–
NH(gly)sym	3373					–	3414			3312	3571; 3198	3286;	–	3288	3281	–	–
CH(his)								3130; 2987	3127; 2984			2998	–	–	3003	3000	–
CH(lys)						3050; 2930	3084; 2920			2975; 2936	2868; 2789 [54]; 2654 [54]	2956 – 2858	– – –	2953 – 2857	2952; – 2857	2953 – 2853	2951; 2901 –
C=O(ester)	1740					1667	1703			1734	1734 [54]; 1634	1741	1758	1733	–	1759*	1753*
C=O(amideI)	1648	–	1657		1648							1647	1641	1652; 1636	1658; **1645**	1652; 1635	1659; **1642**
HNH bend						–	1610			–	1619 [54]; 1554; 1525 [54];	–	1635	1646	1651	1646	–
CNH(amideII)	1551		1563		1586							– 1490	1586; 1488	1582; 1489	**1584;** –	1576; 1488	**1585;** 1481
C=C(His)		1568	–	1569				1573	1575			1573	1569	1569	1564	1568	1565
C=N(His)								1490	1490			–	–	1497	1496	1496	1493
HCH scis.						1410	1410	1451	1451		1475 [54]; 1462 [54]; 1445 [54]	1476; 1446	1441	1464; 1457	1468; 1455	1472; 1456*	1461; 1450*
C–N(His)		–	1104; 1086	–	1105; 1084			1424; 1085	1423; 1087			1097	1093	1435; 1090	1435; 1089	1425*; 1092*	1435; 1088*
NH2twist+CH2twist						1323	1334			1352	1355 [54]	1352	–	1351	1352	1362	1357
$\nu_{CN(ring)}+\delta_{NCH(ring)}$		1267	–	1267	–			1301	1304			1268	1264	1265	1266	1275*	1268
CN (amideIII)												1246	1239	1241	**1241**	–	**1231**
$\delta_{CNC(ring)}+\nu_{CN(His)}$								975	975			990	986	985	984	–	–
$\delta_{NCN(ring)}+\delta_{CNC(ring)}$								935	941			938	–	948	947	956*	947
$\Gamma_{CNCH(ring)}$									764			781	772	777	776	749*	746*
$\Gamma_{NCCH(ring)}$												–	–	681	681	–	–
$\delta_{CCO\ (Carboxyl)}$												–	656; 507	652; 506	651; 499	–	660 503
$\Gamma_{COOH(Carboxyl)}$							584					–	573	570	575	568	576

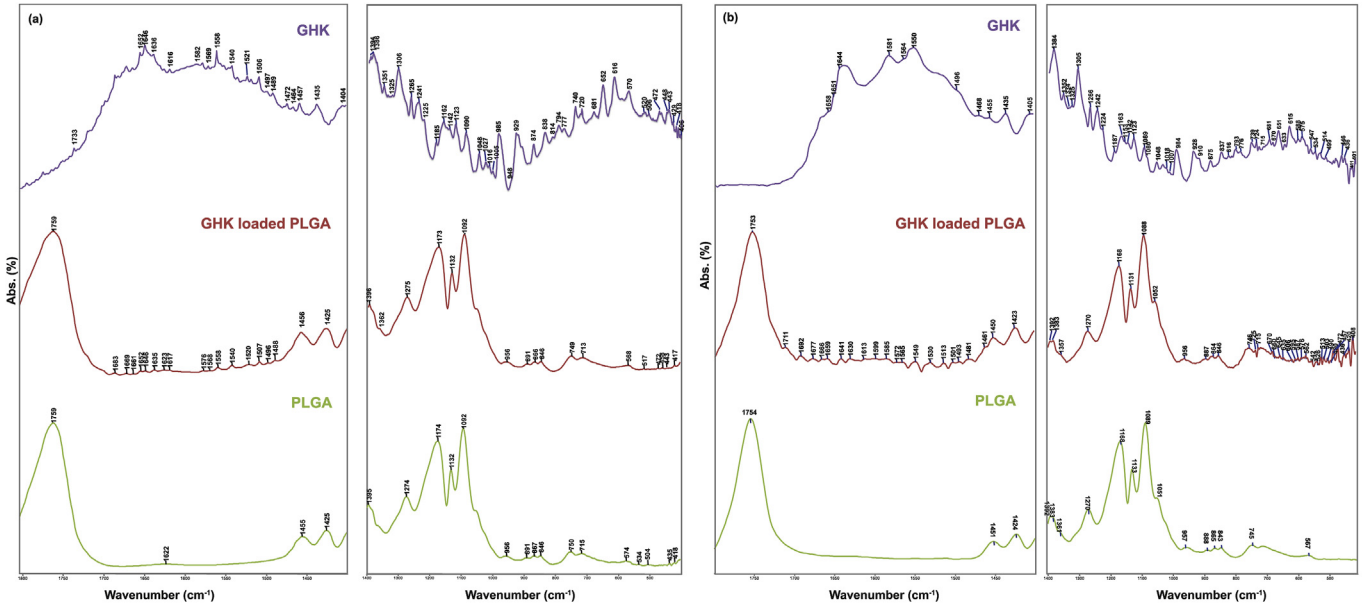

Fig. 4. The comperative FT-IR spectra of GHK tripeptide, PLGA NPs and GHK-loaded PLGA NPs in the region of 1800 - 400 cm^{-1} (a). The comperative ATR spectra of GHK tripeptide, PLGA NPs and GHK-loaded PLGA NPs in the region of 1800 - 400 cm^{-1} (b).

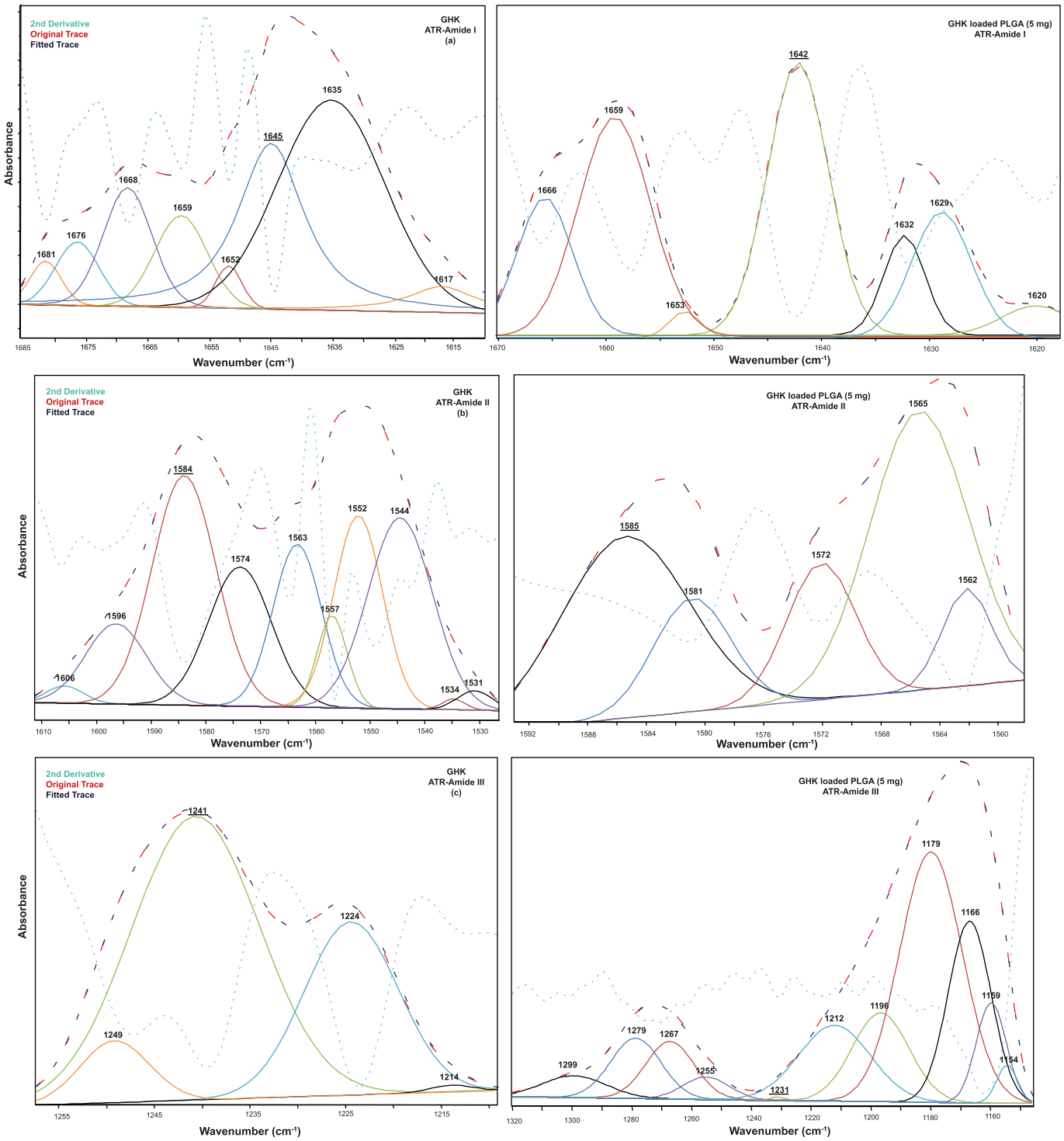

Fig. 5. The band component analysis of amide I, 1686-1610 cm^{-1} and 1670-1618 cm^{-1} region of the ATR spectrum of GHK and GHK-loaded PLGA NPs (a). The band component analysis of amide II, 1611-1526 cm^{-1} and 1593-1558 cm^{-1} region of the ATR spectrum of GHK and GHK-loaded PLGA NPs (b). The band component analysis of amide III, 1257-1209 cm^{-1} and 1320-1145 cm^{-1} region of the ATR spectrum of GHK and GHK-loaded PLGA NPs (c).

GHK-loaded NP spectra, respectively. The vibration of the CNCC (ring) characterizing the histidine part was observed at 615 cm^{-1} in Fig. 4b, whereas for 10 mg GHK-loaded PLGA NP spectra, it was observed at 613 cm^{-1} with 2 cm^{-1} shift, this band have been recorded very low intensity for 5 mg and 20 mg GHK-loaded NP spectra in Fig. S2. The band corresponding to the $\delta_{CCN} + \delta_{CCO}$ in Table 2 observed at 588 cm $^{-1}$in Fig. 4b was determined at 587 cm $^{-1}$ for 5 and 10 mg GHK loaded, for 20 mg GHK-loaded NP with lower intensity. The torsion COOH and angle bending CCO vibrations of the carboxyl group were determined at 575 and 499 cm^{-1}, respectively, for the GHK tripeptide in Fig. 4b and Table 2. These vibrational wavenumbers are shifted to 576, 503 cm^{-1} with 1 and 4 cm^{-1} shifts for 5 mg GHK-loaded; to 570, 498 cm^{-1} with 5 and 1 cm^{-1} shifts for 10 mg GHK-loaded; to 566, 498 cm^{-1} with 9 cm^{-1}

and 1 cm^{-1} for the 20 mg GHK-loaded, were observed in Fig. S2. In addition, the band belonging to the ring and corresponding to the NCNH torsional vibration was determined at 534 cm^{-1} for GHK in Fig. 4b. In the NP spectra for 5, 10 and 20 mg loaded as a result of encapsulation, this band was formed by 8, 4 and 7 cm^{-1} shifts at 526,530 and 527 cm^{-1} respectively in Fig. S2. Besides, the angle bending vibration of the carboxyl group (COH) of the GHK tripeptide was determined at 1340 cm^{-1} in Table 2. However, for 20 mg GHK-loaded PLGA spectra, this band was clearly observed at 1338 cm^{-1}, whereas for 10 mg and 5 mg GHK-loaded, it was observed to be lower intensity in Fig. S3.

3.6. MD results

To determine the effect of the solvent medium on conformation, the geometry of the 944 mol water molecule and the 444 mol of methanol molecule and the optimized Gly-Lys-His tripeptide was placed in a cubic box, and also a sufficient number of ions were added to the system to ensure neutralization in Fig. 6. To provide the proper geometry of the systems, the steepest-descent algorithm was carried out with a 50000-step for energy minimizations and energies were converged to -4.324×10^4 kJ/mol ve -1.51×10^4 kJ/mol for water and methanol systems, respectively in Fig. S4. The NVT and NPT ensembles were carried out for 25,000 and 250,000 steps with a 2 fs time to fixed the temperature and pressure to 300K and 1 bar, respectively. The average density value 987.86 kg m-3 of the system was obtained after NPT simulation in Fig. S5. The RMSD (Root Mean Square Devination)and Rg (Radius of Gyration)values of the systems were calculated as a result of MD calculation which was calculated as 10 ns with 5,000,000 steps. For water system, the RMSD value was found to be in the range of 0.17–0.01 nm and for methanol medium system, this value was limited to be in the range of 0.011 nm and 0.16 nm during the simulation. RMSD gives an idea of how similar of our system is to the first geometric structure, and this value is expected to be approximately 0.2 nm or less, indicating that the peptide remains in its initial form throughout the simulation [56]. The RMSD values calculated for both systems were below 0.2 nm and the molecular structure of the tripeptide in the medium systems remained in the geometries close to the first optimized geometry without degradation. The radius (Rg) of the peptide was calculated during the simulation for 10 ns, and the results of Rg calculations consistent with RMSDs are shown in Fig. S6. The compatibility of RMSD with the literature indicates that GHK tripeptide in the different mediums (water and methanol) maintains the stability of the tripeptide.

3.7. HOMO-LUMO and UV–Vis analysis results

The calculated absorption wavelengths λ(nm), excitation energies E (eV), and oscillator strengths (f) of GHK tripeptide along with transition levels and the major contribution on molecular orbitals for various mediums (methanol, distilled water) and gas medium were tabulated in Table 4(a). The values of obtained λ and E (eV) using **TD-B3LYP/6-311++G(d,p) basis set** are 228.12, 224.73, 224.05 nm and 5.43, 5.51,5.53 eV for methanol medium, 228.13, 224.8, 223.9 nm and 5.43, 5.51,5,53 eV for water and 234.66, 231.33, 231.26 nm and 5.28, 5.35, 5.36 eV for gas medium respectively as

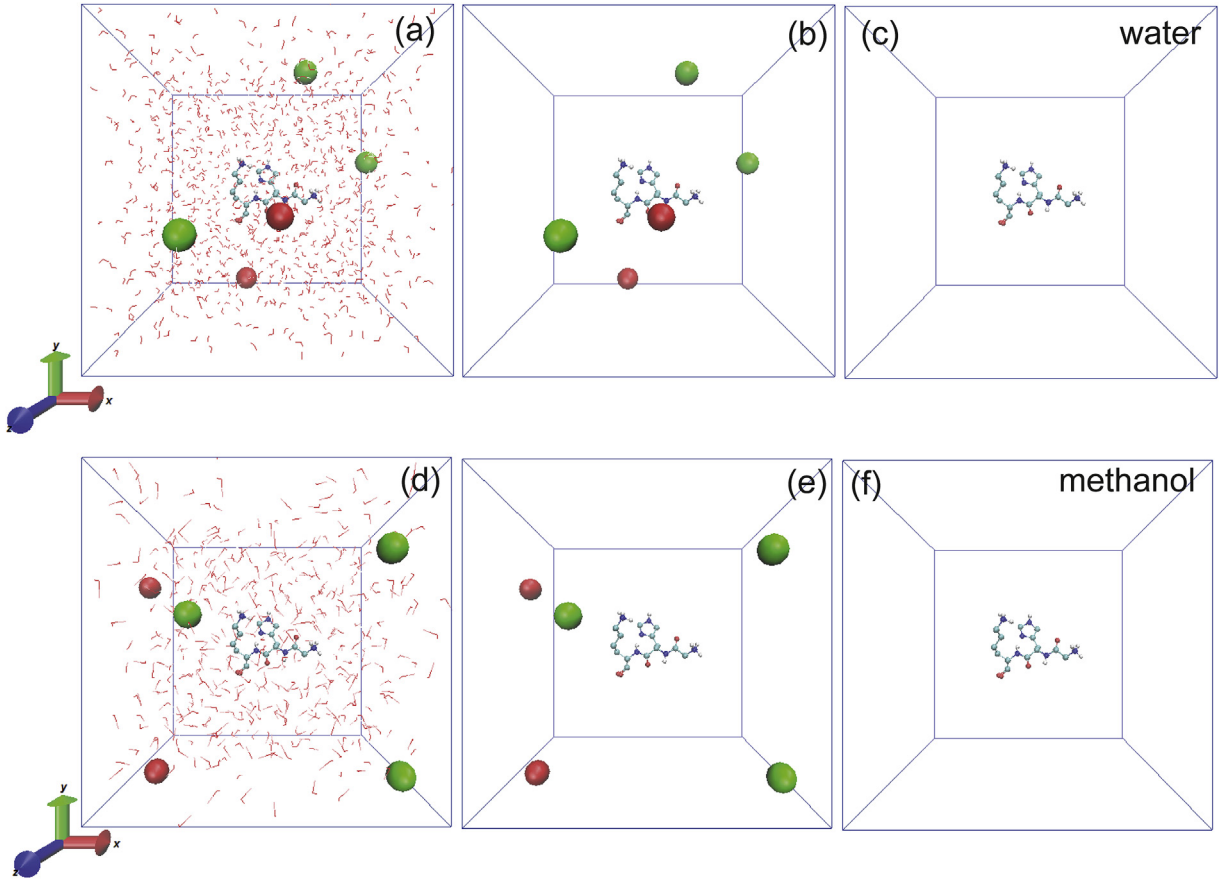

Fig. 6. Gly-His-Lys tripeptide in a cubic box solvated with 944 SPC water molecules and 5 ions (a), in a cubic box neutralized with 2 Na+ and 3 Cl-ions (b), and initial conformation. (c). Gly-His-Lys tripeptide in a cubic box solvated with 444 methanol molecules and 5 ions (d), in a cubic box neutralized with 2 Na+ and 3 Cl-ions (e), and initial conformation (f).

shown in Fig. S7(a). The most important contribution to molecular orbitals was the presence of methanol and water medium with the contribution of 56% from HOMO-3 to LUMO, while 81% contribution from HOMO-2 to LUMO was obtained for gas medium using GaussSUM program. The experimentally obtained absorption wavelength and excitation energies of GHK tripeptide in methanol and water solutions are 225 nm and 216.5 nm and 5.51 eV and 5.72 eV in Fig. S7(b), also tabulated in Table 4(b) respectively. As can be seen from the tables, the experimental and theoretically calculated wavelength values as well as the excitation energy values are in harmony especially for the methanol medium and are valid even though there are small differences ($\Delta\lambda_{calc.-exp} = 7{,}4$ nm and $\Delta E_{calc.-exp} = 0.19$ eV) in the water medium. The calculated molecular orbital energies (eV), HOMO–LUMO band gaps obtained by TD-DFT/6–311++G(d,p) basis set tabulated and also listed in Table 5. In the gas medium, HOMO that represents the ability to donate electron is located over the glycine region with −6.5925 eV energy and LUMO is capable of receiving electron and settled in over the histidine ring with −0.67185 eV energy. The calculated band gap ($\Delta E_{HOMO-LUMO}$) energy was −5.92 eV. For the methanol and water medium, the HOMO and LUMO are identical sites, while the HOMO orbitals are in the histidine region and the LUMO orbitals are on the Lysine amino acid, the carboxyl group and peptide group. The band gap values obtained for both mediums are close to each other (−6.038 eV and-6.032eV for methanol and water) see Fig. S8. The HOMO–LUMO transition indicated that charge transfer occurred from the imidazole ring in the histidine part to the carboxyl groups and peptide group of the Lysine moiety. The calculated values of ionization potential, electron affinity, chemical hardness values for various mediums (methanol, distilled water) and gas medium of GHK tripeptide were tabulated in Table 6. As can be seen from Table 5, in the gas medium having the lowest chemical hardness (2.9603eV), the band gap energy is lower (5.9206 eV) than other medium, GHK tripeptide is more active and reactive, whereas in the methanol medium, GHK tripeptide has higher chemical hardness (3.0193 eV), the band gap (6.0387 eV) is larger and the molecular structure is more stable.

3.8. MEP analysis results

The MEP analysis for GHK tripeptide in various mediums (methanol and water) and gas phase were calculated and shown in Fig. S9. The potential energy values were determined as ±0.07279 a. u., ±0.08623 a. u. and ±0.08587 a. u. for gas phase, water and methanol mediums, respectively. The negative potentials were localized on the oxygen atoms (O_8 and O_{25}) of the peptide bonds with −0.0509855 a. u., −0.0504291 a. u. energies for gas, −0.0570572 a. u., −0.057372 a. u. energies for water and −0.0568727 a. u., −0.057338 a. u. energies for methanol solutions. Other negative regions are oxygen atom (O46) of carboxyl and nitrogen atom (N_2) of glycine amino acid, and their values are −0.0488796 a. u. and −0.0502025 a. u.,-0.0558071 a. u. and −0.0536127 a. u., −0.0556293 a. u.and −0.0535199 a. u. for gas, water and methanol mediums, respectively. The deepest blue region localized on hydrogen atoms (H_{21} on ring of histidine and H_{48} of the carboxyl group) with a values of +0.0725282 a. u. and +0.054461 a. u. for gas phase, +0.085839 a. u.and +0.0604164 a. u. for water solution and +0.084866 a. u. and +0.0601945 a. u. energy for methanol medium. The results show that the abundance of electrons localized over the electronegative atoms such as oxygen atoms of carboxyl group and oxygen atoms of peptide bonds. Conversely, the absence of the electron region is localized on the ring of Histidine amino acid. The nucleophilic regions localized on the H atoms show the strongest attraction, while the electrophilic regions localized on the O and N atoms show the strongest repulsive effect.

3.9. Molecular docking results

In this study, the docking analysis of GHK tripeptide onto a

Table 4
Calculated and experimentally obtained absorption wavelengths and absorbance values of GHK tripeptide.

(A) Calculated absorption wavelengths λ (nm), excitation energies E (eV), and oscillator strengths (f) of GHK tripeptide along with transition levels and assignments in various mediums.

TD-B3LYP/6–311++G(d,p)					
	E(eV)	λ (nm)	f	Major contribution	
Methanol	5.4351	228.12	0.0025	H-3→L	(56%)
	5.5171	224.73	0.0006	H→L+1, H→L	(33%)
	5.5337	224.05	0.0007	H-2→L+1	(36%)
dH_2O	5.4348	228.13	0.0025	H-3→L	(56%)
	5.5152	224.80	0.0006	H→L	(38%)
	5.5374	223.90	0.0006	H-2→L+1	(41%)
Gas	5.2836	234.66	0.0006	H-2 → L	(81%)
	5.3596	231.33	0.0107	H-1→ L+1	(29%)
	5.3612	231.26	0.001	H → L+5	(28%)

(B) Experimentally obtained absorption wavelength λ (nm), excitation energies E (eV), and absorbance values of GHK tripeptide in methanol and water mediums.

	E (eV)	λ (nm)	Abs.
Methanol	5.5104	225.00	3.085
dH_2O	5.7267	216.50	3.245

Table 5
Calculated molecular orbital energies (eV) and energy differences of GHK tripeptide with TD-DFT/6–311++G(d,p) basis set.

	E_{LUMO+2}	E_{LUMO+1}	E_{LUMO}	E_{HOMO}	$\Delta E_{HOMO-LUMO}$	$\Delta E_{(HOMO)-(LUMO+1)}$	$\Delta E_{(HOMO)-(LUMO+2)}$
Gas	−0.3015	−0.4052	−0.6718	−6.5925	**−5.9206**	−6.1873	−6.2910
Methanol	−0.1964	−0.3956	−0.5600	−6.5987	**−6.0387**	−6.2031	−6.4023
dH_2O	−0.1975	−0.3994	−0.5676	−6.5998	**−6.0322**	−6.2004	−6.40232

Table 6
The calculated values of ionization potential, electron affinity, and HOMO−LUMO gaps for GHK tripeptide.

Methanol	TD-DFT/6−311++G(d,p)	Energy (a.u.)	Energy (eV)
Homo Energy	E_{HOMO}	−0.24250	−6.5987
Lumo Energy	E_{LUMO}	−0.02058	−0.5600
Ionization Potential	I= - E_{HOMO}	0.24250	6.5987
Electron Affinity	A= - E_{LUMO}	0.02058	0.5600
Electronegativity	χ= (I+A)/2	0.13154	3.5793
Chemical Potential	μ = -(I+A)/2	−0.13154	−3.5793
Chemical Hardness	η = (I−A)/2	0.11096	3.0193
ΔE (gap)	E_{LUMO} - E_{HOMO}	0.22192	6.0387
dH_2O	TD-DFT/6-311++G(d,p)		
Homo Energy	E_{HOMO}	−0.24254	−6.5998
Lumo Energy	E_{LUMO}	−0.02086	−0.5676
Ionization Potential	I= - E_{HOMO}	0.24254	6.5998
Electron Affinity	A= - E_{LUMO}	0.02086	0.5676
Electronegativity	χ= (I+A)/2	0.1317	3.5837
Chemical Potential	μ = -(I+A)/2	−0.1317	−3.5837
Chemical Hardness	η = (I−A)/2	0.11084	3.0161
ΔE (gap)	E_{LUMO} - E_{HOMO}	0.22168	6.0322
Gas	TD-DFT/6-311++G(d,p)		
Homo Energy	E_{HOMO}	−0.24227	−6.5925
Lumo Energy	E_{LUMO}	−0.02469	−0.6718
Ionization Potential	I= - E_{HOMO}	0.24227	6.5925
Electron Affinity	A= - E_{LUMO}	0.02469	0.6718
Electronegativity	χ= (I+A)/2	0.13348	3.6321
Chemical Potential	μ = -(I+A)/2	−0.13348	−3.6321
Chemical Hardness	η = (I−A)/2	0.10879	2.9603
ΔE (gap)	E_{LUMO} - E_{HOMO}	0.21758	5.9206

fibroblast growth factor receptor 2 (pdb code: 5EG3) and also fibroblast growth factor 2 (pdb code: 4OEE), vascular endothelial growth factor receptor 2(pdb code: 3VO3) and DNA topoisomerase II (pdb code: 1ZXM) were implemented and shown in Table 7 and Fig. 7 (a−d). The FGFR2 gene provides instructions for the formation of the protein known as fibroblast growth factor receptor 2, which has important functions such as cell division, regulation of cell growth, formation of blood vessels, wound healing and embryonic development [57,58]. Vascular endothelial growth factor (VEGF) is also very important for tumor angiogenesis and is an effective therapeutic for cancer treatment [59]. Type IIA DNA topoisomers play an important role in the management of DNA structure, modulation of the topological state, chromosome separation and chromatin condensation [60]. Molecular docking analyzes were performed to reveal the effect of GHK on proteins that have such important functions for the body. By linking the GHK tripeptide with different proteins in the different conformations, binding energies were revealed and the most possible binding energies were calculated at −7.513 kcal/mol, −2.188 kcal/mol, −7.437 kcal/mol and −7.238 kcal/mol for proteins (5EG3, 4OEE, 3VO3 and 1ZXM pdb codes), respectively in Table 7. In the active region of the protein (in Fig. 8) in which the GHK tripeptide interacts with, the green, blue, dark blue and orange colored parts represent regions of hydrophobic, polar, positively charged and negatively charged amino acids, respectively. The strong hydrogen bonds and salt bridges formed resulted in the formation of stable binding poses between GHK tripeptideand proteins. As shown Fig. 8a, and Fig. S10a the hydrogen bonds formed with LEU-43 (2.15 Å), LYS-73 (2.26 Å), ALA-123 (2.22 Å), ASN-187 (2.34 Å) and ASP-200 (1.79 Å) residues for fibroblast growth factor receptor 2 (5EG3. pdb). The hydrogen bonds take part between ASN-36 (2.42 Å), ARG-129 (1.95 Å), LYS-144 (1.95 Å)and LYS-134 (2.03 Å) residues and in the active region of fibroblast growth factor 2 (4OEE.pdb) in Fig. 8b, and Fig. S10b. With 5 hydrogen bonds with LEU-37 (1.73 Å), LEU-37 (2.03 Å), ASN-120 (2.09 Å), LYS-117 (1.62 Å) and CYS-116(1.67 Å) of the GHK were firmly coupled to the protein and formed a stable structure for vascular endothelial growth factor receptor 2 (3VO3. pdb) in Fig. 8c, and Fig. S10c.In addition, the connection of GHK with DNA topoisomerase II was shown in Fig. 8d, and Fig. S10d. As can be seen from the figure, ASP-66 (1.91 Å), GLU-59(1.94 Å), ALA-139 (1.82 Å), LYS-140 (2.28 Å), SER-121(2.12 Å) and ASN-122(1.98 Å) hidrogen bondings provide a stable binding pose**.** The N-terminal moiety of the GHK tripeptideinteracts with the polar (ASN-187) and negatively charged (ASP-200) amino acids of the active site of fibroblast growth factor receptor 2 (5EG3. pdb), while the lysine moiety at the C-terminus interacts with hydrophobic (LEU-43) and negatively charged (GLU-130) amino acids. However, the Oxygen atom in the peptide group

Table 7
The conformation and docking score energies between GHK tripeptide and receptor proteins (5EG3, 4OEE, 3VO3 and 1ZXM).

5EG3				4OEE	3VO3	1ZXM
Ligand	Conf.Energies (kcal/mol)	Docking Score (kcal/mol)	Relative dif.	Docking Score (kcal/mol)	Docking Score (kcal/mol)	Docking Score (kcal/mol)
1	**17.971**	***−7.513***	–	***−2.188***	***−7.437***	***−7.238***
2	18.719	−7.126	0.387	−2.056	−7.085	−7.128
3	17.075	−7.043	0.47	−2.022	−6.914	−7.115
4	14.745	−6.795	0.718	−2.013	−6.842	−7.069
5	14.862	−6.762	0.751	−1.860	−6.762	−6.977
6	17.754	−6.441	1.072	−1.853	−6.577	−6.911
7	24.500	−6.425	1.088	−1.739	−6.504	−6.738
8	17.835	−6.329	1.184	−1.722	−6.258	−6.725
9	24.616	−6.267	1.246	−1.527	−6.169	−6.437
10	19.576	−6.196	1.317	−1.482	−6.095	−6.394
11	20.376	−6.135	1.378	−1.459	−6.060	−6.240
12	15.008	−6.112	1.401	−1.390	−6.027	−6.218
13	15.921	−6.091	1.422	−1.369	−6.001	−6.151
14	19.042	−5.964	1.549	−1.332	−5.880	−6.120
15	27.760	−5.816	1.697	−1.131	−5.742	−5.972
16	15.552	−5.775	1.738	−1.065	−5.506	−5.770
17	8.835	−5.771	1.742	−1.026	−5.499	−5.702
18	19.608	−5.742	1.771	−0.755	−5.436	−5.633
19	12.605	−5.387	2.126	−0.751	−5.342	−5.550
20	10.944	−5.328	2.185	−0.728	−5.206	−5.513
21	12.771	−5.318	2.195	−0.604	−5.048	−5.249
22	23.391	−5.293	2.22	−0.486	−4.916	−5.081
23	16.270	−5.043	2.47	−0.369	−4.299	−5.051
24	20.556	−4.365	3.148	−0.178	−3.773	−4.632

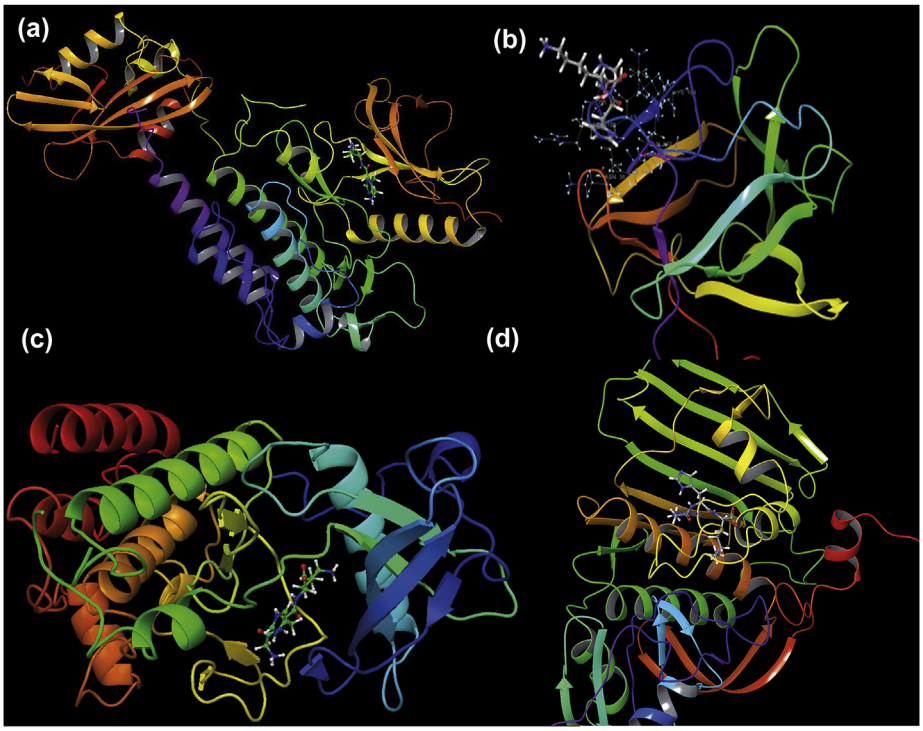

Fig. 7. The binding poses between the active site of the receptors 5EG3 (a), 4OEE (b), 3VO3 (c) and 1ZXM(d) and GHK tripeptide.

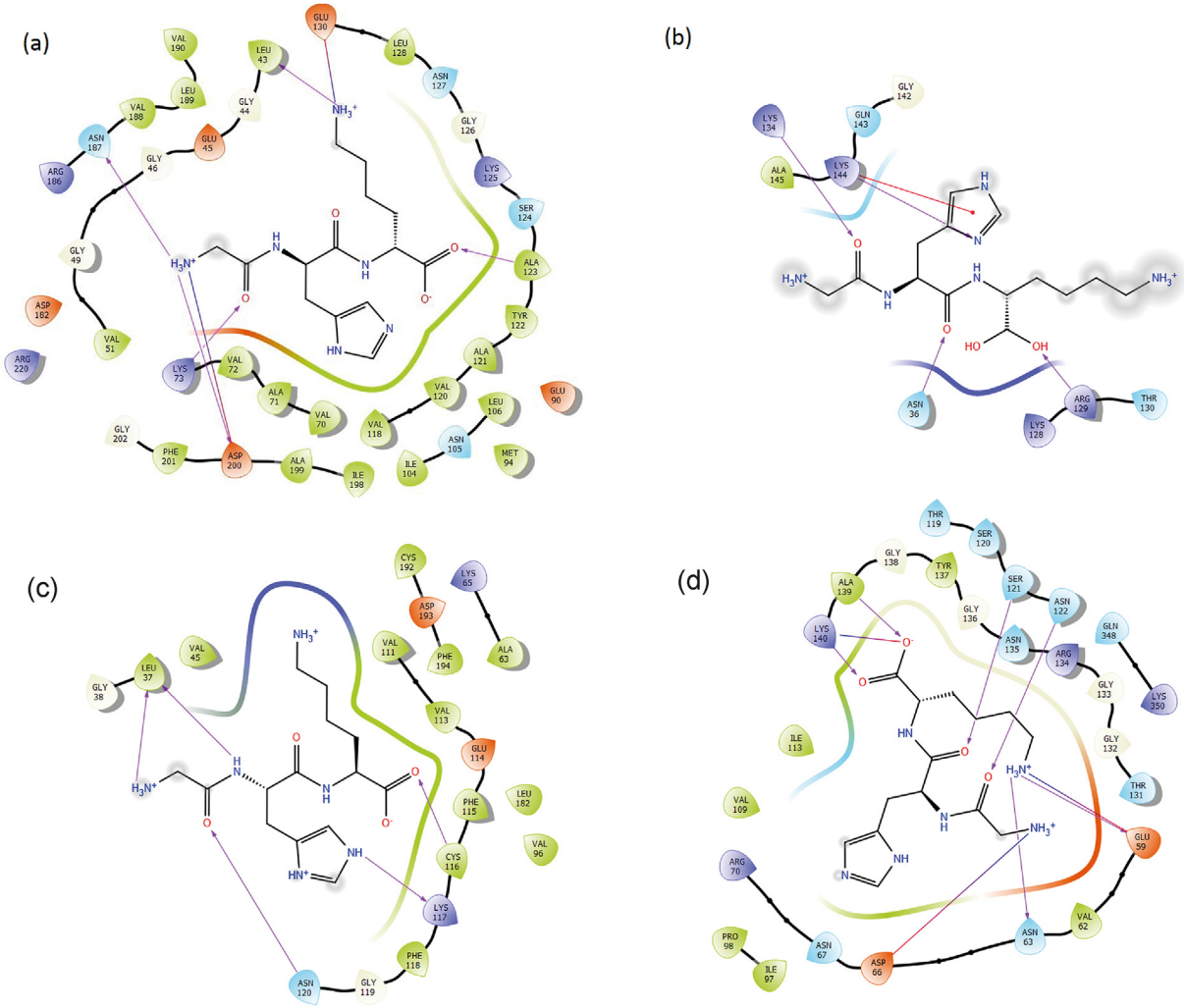

Fig. 8. 2D ligand interaction of GHK tripeptide in the active site of the proteins 5EG3 (a), 4OEE (b), 3VO3 (c) and 1ZXM (d).

is linked to the positively charged amino acid (LYS-73) and the Oxygen atom in the carboxyl group was also bound with the hydrophobic amino acid (ALA-123). The salt bridges between the tripeptide and the protein structure are formed by the close electrostatic interaction of the amino acids with the opposite charge. Both salt bridges were formed between the positively charged NH_3^+ group (at the N-terminal end and the Lysine amino acid) and the negatively charged amino acids (ASP-200 and GLU-130) located at the active region of the fibroblast growth factor receptor 2 (5EG3. pdb) in Fig. 8a. The active site of fibroblast growth factor 2 (4OEE.pdb) protein consists of positively charged amino acid residues (ARG-129, LYS-128, LYS-144 and LYS-134), polar (GLN-143, ASN-36, THR-130) residues and hydrophobic (ALA-145)residues.In addition, a salt bridge was formed also between the N atom of histidine and LYS-144 in Fig. 8b. As shown in Fig. 8c, the active binding region of VEGF (3VO3) has hydrophobic residues (LEU-37, CYS-116, PHE-118, VAL-45, VAL-113, VAL-111), polar (ASN-120) and positively charged (LYS-117) residues. Furthermore, the active binding region of DNA topoisomerase II interacts with negatively charged (GLU-59, ASP-66), polar (ASN-63, ASN-122, SER-121), positively charged (LYS-140, ARG-134) and hydrophobic (ALA-139) residues in Fig. 8d. Electrostatic potential surfaces are important in computer-aided drug design; as these surfaces identify electron-rich and electron-poor regions and provide information about the electrostatic interaction and electron transitions between the protein and the ligand. While the red surfaces (ASP-200, GLU-130) correspond to the electron-rich,electrophilic, region in protein which defines the lowest electrostatic potential energy value interacted by nucleophilic region (NH_3^+ group) of GHK tripeptide, the dark blue (LYS-73) surface in protein defines the nucleophilic region with the electron deficiency interacted by electrophilic atom (O), showing the highest electrostatic potential energy value in Fig.S11 The electrostatic potential surface areas of fibroblast growth factor 2 (pdb code: 4OEE), vascular endothelial growth factor receptor 2 (pdb code: 3VO3) and DNA topoisomerase II (pdb code: 1ZXM) were obtained and GHK tripeptide docked poses in these areas were also shown in Fig. S11.

3.9.1. ADME results

The ADME profile, in which the pharmacokinetic properties of a substance are determined by Qikprop tool of the Maestro software, are as follows. Absorbtion (A); (Bioavailability) defines the amount of drug absorbed per unit time (Mw, small intestine absorption), Distribution (D); transition of the drug from the blood circulation to the intracellular space or cells, Metabolism (M); describes the separation of metabolites of the compounds in the body and breakthrough, Excretion (E); describes the excretion of compounds and metabolites through the kidney, intestine and lung. Pharmacokinetic parameters which are required for predicting the drug-like properties of molecules; were listed in Table 8. According to the Lipinski 5s rule; the molecular weight should not be greater than 500 Mw, no more than 5 hydrogen bond donors, no more than 10 hydrogen bond acceptors, and the octanol/water partition coefficient should not be greater than 5. GHK tripeptidehas 340 g/mol molecular weight, 6 hydrogen bond donors and 9 hydrogen bond acceptors, and the calculated value of octanol/water partition coefficient is −3.868. The rate of skin permeability (SP) is a very important pharmacokinetic property for the transdermal effect of drugs and cosmetics, especially in the fields of medicine and cosmetics [61]. It is very important to know this property for GHK andits copper complex, increase stem cell regeneration in the skin, used in many cosmetic products, since they provide new vessel formation. The calculated QP log Kp for skin permeability (Kp in cm/hr) value of GHKtripeptide is −9.697.

Kp is given as following formula [62],

$$K_p = \frac{K_m \times D}{h} \tag{6}$$

where K_m is distribution coefficient between stratum corneum and vehicle, and D is average diffusion coefficient (cm^2/h), and h is thickness of skin (cm). According to the results of the in vivo study performed, GHK tripeptidehas also been tested and accepted on rats with anti-anxiety, anti-pain and anti-aggression properties [63]. It is important to know the ability to cross the blood brain barrier due to its anti-anxiety activity. The calculated brain/blood partition coefficient (QPlogBB) is −2.441 and is within the recommended range of value (−3.0 − 1. 2). Additionally, Human serum albumin (HSA) is important like the blood-brain barrier for the probability of being drug. Interactions of HSA and small molecules affect the ADME properties which calculated for small molecules [64,65]. QP log K hsa Serum Protein Binding value was determined as −1.556 (standard limits from −1.5 to 1.5).

Table 8
Docking score and calculated ADME properties of GHK tripeptide with 5EG3 protein.

Property	Value	Recommended
Docking score (kcal/mol)	−7.513	
Polar surface area PSA (Å2)	197.821	7.0/200.0
Molecular Weight, MW (g/mol)	**340.381**	**130.0/725.0**
QP Polarizability (Angstromŝ3)	30.663M	(13.0/70.0)
QP log P for hexadecane/gas	12.735M	(4.0/18.0)
QP log P for octanol/gas	**25.070M**	**(8.0/35.0)**
QP log P for water/gas	21.918M	(4.0/45.0)
QP log P for octanol/water	−3.868	(−2.0/6.5)
QP log S for aqueous solubility	0.515	(−6.5/0.5)
QP log S - conformation independent	0.636	(−6.5/0.5)
QP log K hsa Serum Protein Binding	−1.556	(−1.5/1.5)
QP log BB for brain/blood	**−2.441**	**(-3.0/1.2)**
No. of Primary Metabolites	8	(1.0/8.0)
Predicted CNS Activity (– to ++)	–	
HERG K+ Channel Blockage: log IC50	−1.760	(concern below −5)
Apparent Caco-2 Permeability (nm/sec)	0	(<25 poor. >500 great)
Apparent MDCK Permeability (nm/sec)	0	(<25 poor. >500 great)
QP log Kp for skin permeability	**−9.697**	**(Kp in cm/hr)**
Jm, max transdermal transport rate	0	(micrograms/cm^2-hr)
Lipinski Rule of 5 Violations	1	(maximum is 4)
% Human Oral Absorption in GI (+-20%)	0	(<25% is poor)

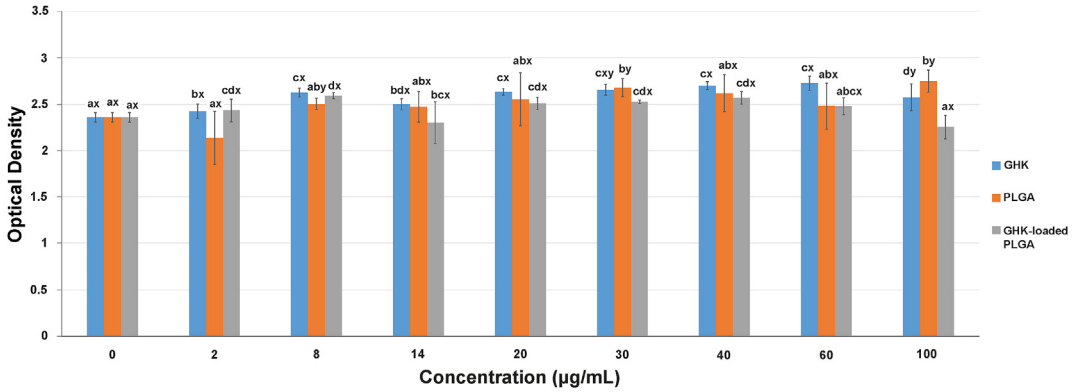

Fig. 9. Effects of GHK, PLGA NPs and GHK-loaded PLGA NPs on L929 cell line. *Each bar is the mean ± standard error of three replicates. *Significant differences are indicated by a–d ($P < 0.05$, Tukey's HSD test) among doses at each time point and x–y ($P < 0.05$, Tukey's HSD test) between time points in the same dose column.

Table 9
The effect of different concentrations of GHK, PLGA nanoparticles and GHK-loaded PLGA nanoparticles on L929 cell viability.

	% Viability		
Concentration (µg/ml)	GHK	PLGA	GHK loaded PLGA
2	103,1	91,0	103,6
8	111,9	106,5	110,4
14	106,4	105,2	97,9
20	112,3	108,6	106,7
30	113,1	114,0	107,5
40	114,9	111,4	109,3
60	114,9	111,4	109,3
100	116,0	105,5	105,4

3.10. Cytotoxicity results

The second generation tetrazolium dye, XTT assay which is based on the reduction of reactant to a colorful product in the presence of mitochondrial enzymes of viable cells, can be effectively used in cell proliferation, cytotoxicity, and apoptosis assays [66,67]. As seen in Fig. 9, there are no toxic effects of GHK, PLGA NPs or GHK-loaded-PLGA NPs in the examined concentrations. The increase in the optical density in proportion to the cell viability is similar to the control in the experimental groups. The optical density values expressed in Fig. 9, are stated as % viability in Table 9. As seen in Table 9, cell viability is above 90% in all groups. According to the ISO 10993-5 standard, cell viability above 80% is expressed as non-toxic [68,69]. Accordingly, the concentrations of GHK, PLGA and GHK-loaded-PLGA NPs are non toxic.

4. Conclusions

GHK tripeptide has an important potential for cosmetic products with wound healing and skin protective properties, besides its antioxidant and antitumor properties. In this study, GHK is encapsulated with an FDA-approved PLGA polymer for the aim faster penetration on the skin, maintaining its stability in the body, enhancing its bioavailability, maintaining its effectiveness for a longer time and ensuring controlled release. *In vitro* cell culture studies of GHK tripeptide and GHK-loaded PLGA NPs were performed and the non-toxic effect on L929 cells was also investigated. Toxicity was not expected for GHK tripeptide because this natural product normally found in the human plasma, saliva and body fluids [1]. PLGA is also non-toxic polymer [19]. According to the toxicity results, the percentage viability of GHK-loaded PLGA NPs are over 80% and they are not toxic. This study supports the development and design of more active products with better effectiveness and stability, especially in skin protective products due to the nano formulation. In addition to these, for the first time GHK tripeptide was modelled by using *in silico* methods and the mechanism of interaction was revealed with the possible receptor that could act within the body. Also, the interaction of PLGA and GHK tripeptide was revealed spectroscopically and the interactions of GHK tripeptide with polymer due to the encapsulation were determined.

Declarations of interest

None.

Acknowledgments

This study consists of the results of the master thesis study and was supported by the Scientific Research Project Coordination Unit of Istanbul University [FYL-2017-25634, ONAP-2423]. Authors are very thankful to Rita Podzuna for allowing to use the docking program with Schrödinger's Small-Molecule Drug Discovery Suite. Authors also would like to thank Dr. Loren Pickart for discovered GHK tripeptide and for gained to the literature. In this study, the infrastructure of Applied Nanotechnology and Antibody Production Laboratory established with TUBITAK support (project numbers: 115S132 and 117S097) was used. Authors would thank to TUBITAK for their support.

Appendix A. Supplementary data

Supplementary data to this article can be found online at https://doi.org/10.1016/j.molstruc.2019.127046.

References

[1] L. Pickart, A Tripepeptide in Human Serum that Promotes the Growth of Hepatoma Cells and the Survival of Normal Hepatocytes, University of California, San Francisco, Calif, USA, 1973.
[2] Cheah, P. Y. Hong, T. Downey, K. Eu, P. Koh, A "metastasis-prone" signature for early-stage mismatch-repair proficient sporadic colorectal cancer patients and its implications for possible therapeutics Clin. Exp. Metastasis 27 (2010) 83–90.
[3] L.E. Matalka, A. Ford, M.T. Unlap, The tripeptide, GHK, induces programmed cell death in SH-SY5Y neuroblastoma cells, J. Biotechnol. Biomater. 2 (2012) 1–4.
[4] L. Pickart, J.M. Vasquez-Soltero, F. Pickart, J.D. Majnarich, GHK, the human skin remodeling peptide, induces anti-cancer expression of numerous caspase, growth regulatory, and DNA repair genes, J. Anal. Oncol. 3 (2) (2014) 79–87.
[5] L. Pickart, A. Margolina, Skin regenerative and anti-cancer actions of copper peptides, Cosmetics 5 (2) (2018) 29.
[6] X.M. Zhou, G.L. Wang, X.B. Wang, L. Liu, Q. Zhang, Y. Yin, et al., GHK peptide inhibits bleomycin-induced pulmonary fibrosis in mice by suppressing TGFβ1/smad-mediated epithelial-to-mesenchymal transition, Front. Pharmacol. 8 (2017) 904.
[7] J. Cebrian, A. Messeguer, R.M. Facino, J.M. García Antón, New anti-RNS and -RCS products for cosmetic treatment, Int. J. Cosmet. Sci. 27 (5) (2005)

271–278.
[8] V. Pešáková, J. Novotná, A. Milan, Effect of the tripeptide glycyl-L-histidyl-L-lysine on the proliferation and synthetic activity of chick embryo chondrocytes, Biomaterials 16 (12) (1995) 911–915.
[9] G. Beretta, E. Arlandini, R. Artali, J.M. Anton, R. Maffei Facino, Acrolein sequestering ability of the endogenous tripeptide glycyl-histidyl-lysine (GHK): characterization of conjugation products by ESI-MSn and theoretical calculations, J. Pharm. Biomed. Anal. 47 (2008) 596–602.
[10] M. Sensenbrenner, G.G. Jaros, G. Moonen, B.J. Meyer, Effect of conditioned media on nerve cell differentiation, Cell. Mol. Life Sci. 36 (1980) 660–662.
[11] H. Zhang, Z. He, Y. Wang, GHK alleviates neuronal apoptosis due to intracerebral hemorrhage via the miR-339-5p/VEGFA pathway, Front. Neurosci. 12 (2018) 644.
[12] M.R. Ahmed, S.H. Basha, D. Gopinath, R. Muthusamy, R. Jayakumar, Initial upregulation of growth factors and inflammatory mediators during nerve regeneration in the presence of cell adhesive peptide-incorporated collagen tubes, J. Peripher. Nerv. Syst. 10 (1) (2005) 17–30.
[13] T.F. Lane, M.L. Iruela-Arispe, R.S. Johnson, E.H. Sage, SPARC is a source of copper-binding peptides that stimulate angiogenesis, J. Cell Biol. 125 (1994) 929–943.
[14] I.I. Bobyntsev, O.I. Chernysheva, M.E. Dolgintsev, M.Y. Smakhtin, A.E. Belykh, Anxiolytic effects of Gly-His-lys peptide and its analogs, Bull. Exp. Biol. Med. 156 (2015) 726–728.
[15] L. Pickart, The human tri-peptide GHK and tissue remodeling, J. Biomater. Sci. Polym. Ed. 19 (8) (2008) 969–988.
[16] L. Sun, A. Li, Y. Hu, Y. Li, L. Shang, L. Zhang, Self-assembled fluorescent and antibacterial GHK-Cu nanoparticles for wound healing applications, Part. Part. Syst. Charact. (2019), 1800420, https://doi.org/10.1002/ppsc.201800420.
[17] Y. Budama-Kilinc, R. Cakir-Koc, G.O. Eren, P.K. Akman, M.T. Yilmaz, Production OF GHK tripeptide embedded poly vinyl alcohol-nanofibers, Feb-Fresenius Environmental Bulletin (2018) 1202.
[18] G. Crotts, Protein delivery from poly(lactic-co-glycolic acid) biodegradable microspheres: release kinetics and stability issues, J. Microencapsul. 15 (1998) 99–713.
[19] C.E. Astete, C.M. Sabliov, Synthesis and characterization of PLGA nanoparticles, J. Biomater. Sci. Polym. Ed. 17 (3) (2006) 247–289, https://doi.org/10.1163/156856206775997322.
[20] D. Van Der Spoel, E. Lindahl, B. Hess, G. Groenhof, A.E. Mark, H.J. Berendsen, J. Comput. Chem. 26 (16) (2005) 1701–1718.
[21] M. Frisch, G. Trucks, H. Schlegel, G. Scuseria, M. Robb, J. Cheeseman, G. Scalmani, V. Barone, B. Mennucci, G. Petersson, Gaussian 09, Revision a. 02, gaussian. Inc., Wallingford, CT, 2009, p. 200.
[22] W.F. van Gunsteren, S.R. Billeter, A.A. Eising, P.H. Hünenberger, P. Krüger, A.E. Mark, W.R. Scott, I.G. Tironi, Biomolecular Simulation: the {GROMOS96} Manual and User Guide, 1996.
[23] P.E. Smith, W.F. van Gunsteren, The viscosity of SPC and SPC/E water at 277 and 300 K, Chem. Phys. Lett. 215 (4) (1993) 315–318.
[24] G. Bussi, D. Donadio, M. Parrinello, Canonical sampling through velocity rescaling, J. Chem. Phys. 126 (1) (2007), 014101.
[25] M. Parrinello, A. Rahman, Polymorphic transitions in single crystals: a new molecular dynamics method, J. Appl. Phys. 52 (12) (1981) 7182–7190.
[26] B. Hess, H. Bekker, H.J. Berendsen, J.G. Fraaije, LINCS: a linear constraint solver for molecular simulations, J. Comput. Chem. 18 (12) (1997) 1463–1472.
[27] T. Darden, D. York, L. Pedersen, Particle mesh Ewald: an N. log (N) method for Ewald sums in large systems, J. Chem. Phys. 98 (12) (1993) 10089–10092.
[28] L. Verlet, Computer "experiments" on classical fluids. I. Thermodynamical properties of Lennard-Jones molecules, Phys. Rev. 159 (1) (1967) 98.
[29] W. Humphrey, A. Dalke, K. Schulten, VMD: visual molecular dynamics, J. Mol. Graph. 14 (1) (1996) 33–38, https://doi.org/10.1016/0263-7855(96)00018-5.
[30] J. Fleming, Frontier Orbitals and Organic Chemical Reactions, Wiley, London, 1976.
[31] M. Raja, R.R. Muhamed, S. Muthu, M. Suresh, Synthesis, spectroscopic (FT-IR, FT-Raman, NMR, UV–Visible), NLO, NBO, HOMO-LUMO, Fukui function and molecular docking study of (E)-1-(5-bromo-2-hydroxybenzylidene) semicarbazide, J. Mol. Struct. 1141 (2017) 284–298.
[32] S. Kecel-Gunduz, B. Bicak, S. Celik, S. Akyuz, A.E. Ozel, Structural and spectroscopic investigation on antioxidant dipeptide, l-Methionyl-l-Serine: a combined experimental and DFT study, J. Mol. Struct. 1137 (2017) 756–770.
[33] D. Van Der Spoel, E. Lindahl, B. Hess, G. Groenhof, A.E. Mark, H.J. Berendsen, GROMACS: fast, flexible, and free, J. Comput. Chem. 26 (16) (2005) 1701–1718.
[34] B. Ramachandran, S. Kesavan, T. Rajkumar, Molecular modeling and docking of small molecule inhibitors against NEK2, Bioinformation 12 (2) (2016) 62.
[35] E. Harder, W. Damm, J. Maple, C. Wu, M. Reboul, J.Y. Xiang, et al., OPLS3: a force field providing broad coverage of drug-like small molecules and proteins, J. Chem. Theory Comput. 12 (1) (2015) 281–296.
[36] Z. Huang, W.M. Marsiglia, U.B. Roy, N. Rahimi, D. Ilghari, H. Wang, et al., Two FGF receptor kinase molecules act in concert to recruit and transphosphorylate phospholipase Cγ, Mol. Cell 61 (1) (2016) 98–110.
[37] G.M. Sastry, M. Adzhigirey, T. Day, R. Annabhimoju, W. Sherman, Protein and ligand preparation: parameters, protocols, and influence on virtual screening enrichments, J. Comput. Aided Mol. Des. 27 (3) (2013) 221–234.
[38] S. Bienert, A. Waterhouse, T.A. de Beer, G. Tauriello, G. Studer, L. Bordoli, et al., The SWISS-MODEL Repository—new features and functionality, Nucleic Acids Res. 45 (D1) (2016) D313–D319.
[39] C.R. Søndergaard, M.H. Olsson, M. Rostkowski, J.H. Jensen, Improved treatment of ligands and coupling effects in empirical calculation and rationalization of p K a values, J. Chem. Theory Comput. 7 (7) (2011) 2284–2295.
[40] R.A. Friesner, R.B. Murphy, M.P. Repasky, L.L. Frye, J.R. Greenwood, T.A. Halgren, et al., Extra precision glide: docking and scoring incorporating a model of hydrophobic enclosure for protein− ligand complexes, J. Med. Chem. 49 (21) (2006) 6177–6196.
[41] R.A. Friesner, J.L. Banks, R.B. Murphy, T.A. Halgren, J.J. Klicic, D.T. Mainz, et al., Glide: a new approach for rapid, accurate docking and scoring. 1. Method and assessment of docking accuracy, J. Med. Chem. 47 (7) (2004) 1739–1749.
[42] T.A. Halgren, R.B. Murphy, R.A. Friesner, H.S. Beard, L.L. Frye, W.T. Pollard, et al., Glide: a new approach for rapid, accurate docking and scoring. 2. Enrichment factors in database screening, J. Med. Chem. 47 (7) (2004) 1750–1759.
[43] F. Ntie-Kang, L.L. Lifongo, J.A. Mbah, L.C.O. Owono, E. Megnassan, L.M.A. Mbaze, et al., In silico drug metabolism and pharmacokinetic profiles of natural products from medicinal plants in the Congo basin, In silico pharmacology 1 (1) (2013) 12.
[44] J.M.L. Martin, C. Van Alsenoy, GAR2PED, A Program to Obtain a Potential Energy Distribution from a Gaussian Archive Record, University of Antwerp, Belgium, 1995.
[45] M. Gümüşderelioğlu, G. Deniz, Synthesis, characterization and in vitro degradation of poly (dl-lactide)/poly (dl-lactide-co-glycolide) films, Turk. J. Chem. 23 (2) (1999) 153–162.
[46] J. Yang, C.H. Lee, J. Park, S. Seo, E.K. Lim, Y.J. Song, S. Haam, Antibody conjugated magnetic PLGA nanoparticles for diagnosis and treatment of breast cancer, J. Mater. Chem. 17 (26) (2007) 2695–2699.
[47] H. Gupta, M. Aqil, R.K. Khar, A. Ali, A. Bhatnagar, G. Mittal, Sparfloxacin-loaded PLGA nanoparticles for sustained ocular drug delivery, Nanomed. Nanotechnol. Biol. Med. 6 (2) (2010) 324–333.
[48] C.D.A.C. Erbetta, R.J. Alves, J.M. Resende, R.F. de Souza Freitas, R.G. de Sousa, Synthesis and characterization of poly (D, L-lactide-co-glycolide) copolymer, J. Biomaterials Nanobiotechnol. 3 (02) (2012) 208.
[49] W. Gallagher, FTIR analysis of protein structure, Course manual Chem 455 (2009).
[50] V. Arul, D. Gopinath, K. Gomathi, R. Jayakumar, Biotinylated GHK peptide incorporated collagenous matrix: a novel biomaterial for dermal wound healing in rats, J. Biomed. Mater. Res. B Appl. Biomater. 73 (2) (2005) 383–391.
[51] A. Schirer, Y. El Khoury, P. Faller, P. Hellwig, Similarities and differences of copper and zinc cations binding to biologically relevant peptides studied by vibrational spectroscopies, JBIC Journal of Biological Inorganic Chemistry 22 (4) (2017) 581–589.
[52] S. Kumar, A.K. Rai, V.B. Singh, S.B. Rai, Vibrational spectrum of glycine molecule, Spectrochim. Acta A Mol. Biomol. Spectrosc. 61 (11) (2005) 2741–2746.
[53] K. Hasegawa, T.A. Ono, T. Noguchi, Vibrational spectra and ab initio DFT calculations of 4-methylimidazole and its different protonation forms: infrared and Raman markers of the protonation state of a histidine side chain, J. Phys. Chem. B 104 (17) (2000) 4253–4265.
[54] J. Herrklotz, Analysis of the Vibrational Spectra of L-Lysine and L-Arginine, 2012 (Doctoral dissertation, University of Vienna).
[55] A. Amiri, H.Z. Zardini, M. Shanbedi, M. Maghrebi, M. Baniadam, B. Tolueinia, Efficient method for functionalization of carbon nanotubes by lysine and improved antimicrobial activity and water-dispersion, Mater. Lett. 72 (2012) 153–156.
[56] D. van der Spoel, Structure and Dynamics of Peptides: Theoretical Aspects of Protein Folding, 1996.
[57] F. Carinci, F. Pezzetti, P. Locci, E. Becchetti, F. Carls, A. Avantaggiato, A. Becchetti, P. Carinci, T. Baroni, M. Bodo, Apert and Crouzon syndromes: clinical findings, genes and extracellular matrix, J. Craniofac. Surg. 16 (3) (2005 May) 361–368.
[58] Z. Huang, W.M. Marsiglia, U.B. Roy, N. Rahimi, D. Ilghari, H.,. Wang, A. Mansukhani, Two FGF receptor kinase molecules act in concert to recruit and transphosphorylate phospholipase Cγ, Mol. Cell 61 (1) (2016) 98–110.
[59] N. Miyamoto, N. Sakai, T. Hirayama, K. Miwa, Y. Oguro, H.,. Oki, S. Yamasaki, Discovery of N-[5-({2-[(cyclopropylcarbonyl) amino] imidazo [1, 2-b] pyridazin-6-yl} oxy)-2-methylphenyl]-1, 3-dimethyl-1H-pyrazole-5-carboxamide (TAK-593), a highly potent VEGFR2 kinase inhibitor, Bioorg. Med. Chem. 21 (8) (2013) 2333–2345.
[60] H. Wei, A.J. Ruthenburg, S.K. Bechis, G.L. Verdine, Nucleotide-dependent domain movement in the ATPase domain of a human type IIA DNA topoisomerase, J. Biol. Chem. 280 (44) (2005) 37041–37047.
[61] S.Z. Kovačević, L.R. Jevrić, S.O.P. Kuzmanović, E.S. Lončar, Prediction of in-silico ADME properties of 1, 2-o-isopropylidene aldohexose derivatives, Iran. J. Pharm. Res. (IJPR): IJPR 13 (3) (2014) 899.
[62] S. Singh, J. Singh, Transdermal drug delivery by passive diffusion and iontophoresis: a review, Med. Res. Rev. 13 (5) (1993) 569–621.
[63] L. Pickart, A. Margolina, Regenerative and protective actions of the GHK-Cu peptide in the light of the new gene data, Int. J. Mol. Sci. 19 (7) (2018) 1987.
[64] L.Z. Benet, D. Kroetz, L. Sheiner, J. Hardman, L. Limbird, Pharmacokinetics: the dynamics of drug absorption, distribution, metabolism, and elimination, Goodman and Gilman's the pharmacological basis of therapeutics (1996) 3–27.
[65] K.W. Lexa, E. Dolghih, M.P. Jacobson, A structure-based model for predicting serum albumin binding, PLoS One 9 (4) (2014), e93323.

[66] F.P. Altman, Tetrazolium salts and formazans, Prog. Histochem. Cytochem. 9 (3) (1976) III–51.
[67] M.V. Berridge, P.M. Herst, A.S. Tan, Tetrazolium dyes as tools in cell biology: new insights into their cellular reduction, Biotechnol. Annu. Rev. 11 (2005) 127–152.
[68] J. López-García, M. Lehocký, P. Humpolíček, P. Sáha, HaCaT keratinocytes response on antimicrobial atelocollagen substrates: extent of cytotoxicity, cell viability and proliferation, J. Funct. Biomater. 5 (2) (2014) 43–57.
[69] ISO. 10993-5:2009 *Biological Evaluation of Medical Devices*. Part 5: Tests for in Vitro Cytotoxicity, International Organization for Standardization, Geneva, Switzerland, 2009.